Engineering Failure Analysis 148 (2023) 107199

Contents lists available at ScienceDirect

Engineering Failure Analysis

journal homepage: www.elsevier.com/locate/engfailanal

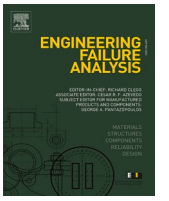

# The fracture behaviour of notched PMMA specimens under simple loading conditions – Tension and torsion experimental tests

Elżbieta Bura [a,*], Andrzej Seweryn [b]

[a] Faculty of Mechanical Engineering, Bialystok University of Technology, Poland
[b] Faculty of Mechanical Engineering and Ship Technology, Gdansk University of Technology, Poland

ARTICLE INFO

*Keywords:*
PMMA
Rounded V-notch
Tension test
Torsion test
Fracture initiation
Crack propagation

ABSTRACT

This paper presents the results of experimental testing of flat PMMA specimens during uniaxial loading conditions. Two separate tests were conducted: tensile and torsion. The specimens were weakened with V-type edge notches with different root radii: 0.5; 2 and 10 mm. The specimens were made in two thickness variants: 5 and 15 mm. Monotonic tensile and torsion tests were carried out while keeping the averaged strain rate constant, due to the strong influence of this parameter on the PMMA behaviour. The procedure for non-contact measurement of the torsion angle using the ARAMIS 3D 4 M vision system is described. A set of PHANTOM cameras was used in the study, thanks to which all fracture processes were recorded. The processing of the obtained recordings made it possible to precisely indicate the moment (critical value of tensile force, torsional moment) and the location of crack initiation, as well as determine the nature of their evolution. Microscopic observations showed the structure of the failure surface and clearly indicated the different initiation sites observed for the two simple loading states. Different crack initiation angles were indicated, depending on the type of test conducted, as well as the notch root radius. The material in the article provides a starting point for numerical modelling of the fracture processes of notched elements and verifying the fracture criteria.

## 1. Introduction

Experimental studies of the fracture of notched plastic components provide insight into the fracture process occurring in these materials. They provide a physical basis for the formulation of computational strength and fracture models of structural polymeric elements. They also facilitate the determination of mechanical properties, in particular, the strength and fracture toughness of specific plastics used in engineering practice. Polymethyl methacrylate (PMMA) which is the subject of the research described in this paper, is used, for example, as a glass substitute in construction and architecture. High impact strength and weather resistance, has also made PMMA widely used in the automotive industry, e.g. for caravan windows, covers in motorcycles, airplanes, helicopters. Its transparency makes it ideal for optical and lighting applications. It has also not been missed in medicine due to the biocompatibility and biodegradability of this material – incubators or laboratory equipment, but also bone prostheses or dental fillings. Wide application of this polymer requires a thorough understanding of its properties.

Plastics are tested in various configurations, in the presence of different notch types and slots, as well as under different operating conditions. Tests presented in the literature are conducted under both simple (monotonic tensile, compression, torsion tests) and

* Corresponding author.
*E-mail addresses:* e.bura@pb.edu.pl (E. Bura), andrzej.seweryn@pg.edu.pl (A. Seweryn).

https://doi.org/10.1016/j.engfailanal.2023.107199
Received 31 January 2023; Received in revised form 2 March 2023; Accepted 14 March 2023
Available online 17 March 2023

**Nomenclature**

| | |
|---|---|
| $\varepsilon$ | Strain, - |
| $\varepsilon_{eng}$ | Engineering strain, - |
| $\varepsilon_{true}$ | True strain, - |
| $\rho$ | Notch root radius, mm |
| $\sigma$ | Stress, MPa |
| $\sigma_{eng}$ | Engineering stress, MPa |
| $\sigma_{true}$ | True stress, MPa |
| $\nu$ | Poisson's ratio, - |
| $\vartheta_0$ | Crack initiation angle, ° |
| $\vartheta_0^{xy}$ | Crack initiation angle on the *xy* plane, ° |
| $\vartheta_0^{yz}$ | Crack initiation angle on the *yz* plane, ° |
| $\dot{\phi}$ | Velocity of angular displacement, °/s |
| $A_0$ | Initial cross-sectional area, mm$^2$ |
| $A_{current}$ | Current cross-sectional area, mm$^2$ |
| $E$ | Young's modulus, MPa |
| $F$ | Tensile force, N |
| $g$ | Nominal specimen thickness, mm |
| $G$ | Shear modulus, MPa |
| $l_0$ | Initial length of the measurement base, mm |
| $R_m$ | Tensile strength, MPa |
| $R_{0.05}$ | Elastic limit, MPa |
| $R_{0.2}$ | Yield strength, MPa |
| $R_u$ | Failure stress, MPa |
| $\bar{k}$ | Normal vector of horizontal symmetry plane of the specimen |

**Table 1**
PLEXIGLAS®GS properties.

| Property | Value | Units |
|---|---|---|
| Young's modulus, $E$ | 3 254 | MPa |
| Tensile strength, $R_m$ | 72.10 | MPa |
| Elastic limit, $R_{0.05}$ | 24.51 | MPa |
| Yield strength, $R_{0.2}$ | 47.17 | MPa |
| Failure stress, $R_u$ | 71.65 | MPa |
| Poisson's ratio, $\nu$ | 0.38 | – |

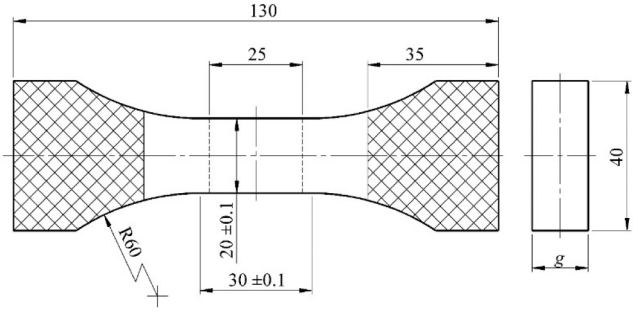


**Fig. 1.** Unnotched specimen (where *g* is a specimen thickness equal to about 5 and 15 mm).

complex loading (monotonic torsion-tensile) conditions. Results of experimental fracture tests of flat specimens with V-type notches of different opening angles and semi-circular notches under uniaxial loading condition are presented in [1]. The typically brittle nature of fracture was observed and the effect of the notch opening angle on the value of the failure load was also analysed. The first type of notch deformation was also realised during three-point bending tests [2] conducted at −60 °C. The test results were used to determine critical load values. Flat elements weakened by a U-notch, made of polycarbonate (PC), were subjected to a four-point bending test and the results are described in the papers [3,4]. The paper [5] describes fracture testing of flat U-notched specimens made of a biopolymer

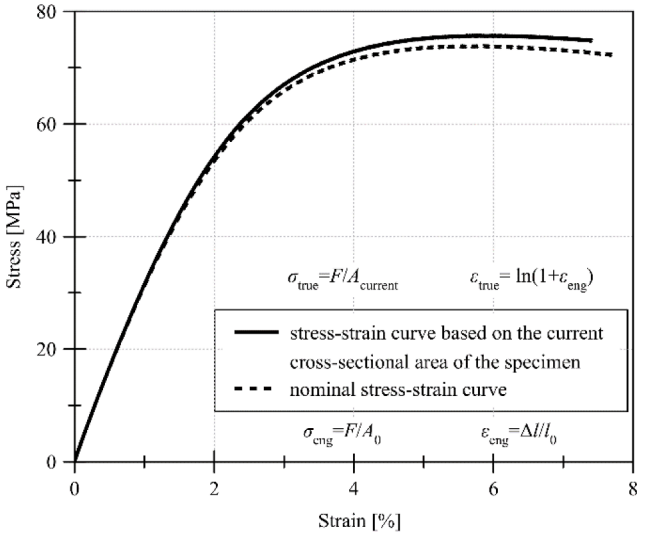


**Fig. 2.** Tensile curves.

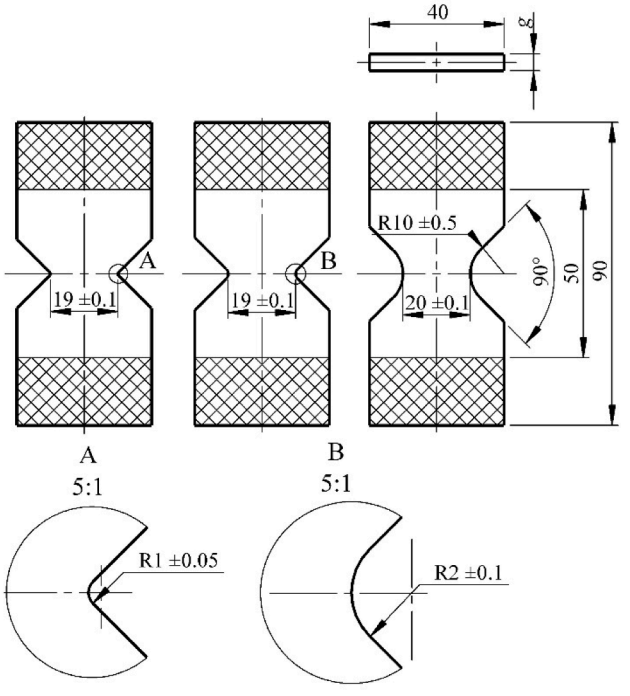


**Fig. 3.** Flat notched specimens used in experimental testing. The hatched area - the surface located in the terminals of the testing machine.

material under monotonic tension. The equivalent material concept was used to predict material fracture. For the case of V-type and U-type notch deformation during the monotonic tensile tests of flat specimens, it was indicated that crack initiation takes place in the symmetry plane of the specimen near its centre of thickness [6]. Researchers also focus on estimating the crack initiation angle, as well as describing the nature of its propagation. The paper [7] describes crack development trajectories for different types of specimens. Attempts have also been made to estimate the speed of crack development for PMMA specimens [6,8,9,10,11]. In all cases, values were obtained at about one-fourth of the sound speed propagation in PMMA [12,13].

Mode III fracture tests were realised during torsion tests of axisymmetric PMMA specimens [14]. The effect of the root radius on the fracture process was studied. The results indicated clear differences in the tensile and torsional behaviour of PMMA. Notched specimens loaded with a torsional moment showed strong plasticity. A marked reduction in plastic deformation was obtained when the same components were tested under torsion at reduced temperature [15]. Simultaneous tearing and transverse shearing of the notches

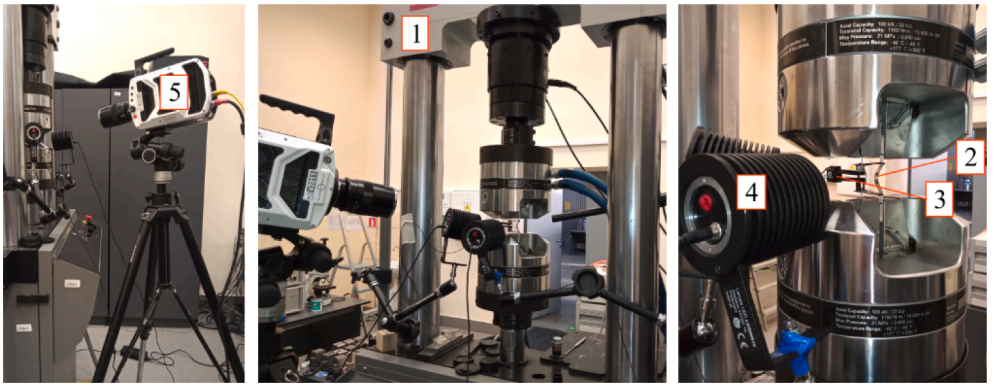


**Fig. 4.** Test stand: 1 - MTS 809.10 testing machine, 2 - specimen, 3 - extensometer, 4 - lamps, 5 - PHANTOM v2210 camera.

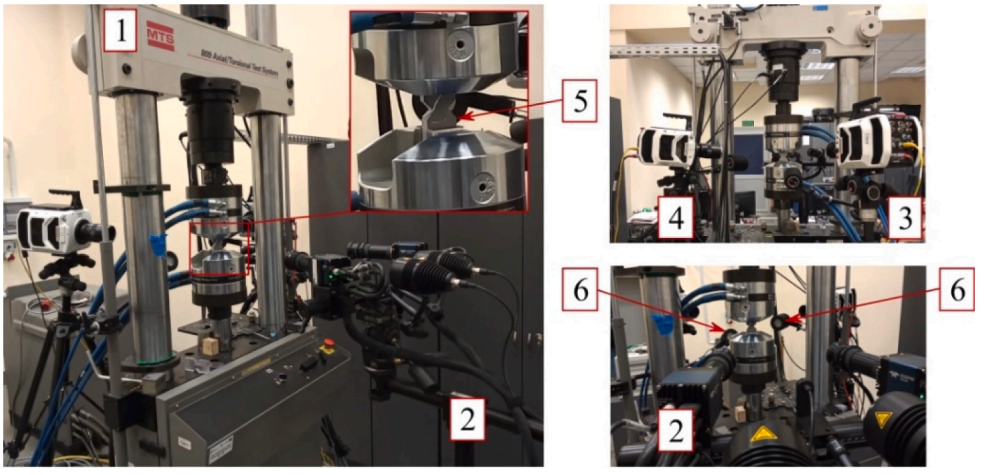


**Fig. 5.** Test stand for fracture testing during torsion: 1 - MTS 809.10 testing machine, 2 - ARAMIS 3D 4 M vision system, 3 - PHANTOM v1610 camera, 4 - PHANTOM v2210 camera, 5 - specimen, 6 - LED lamps.

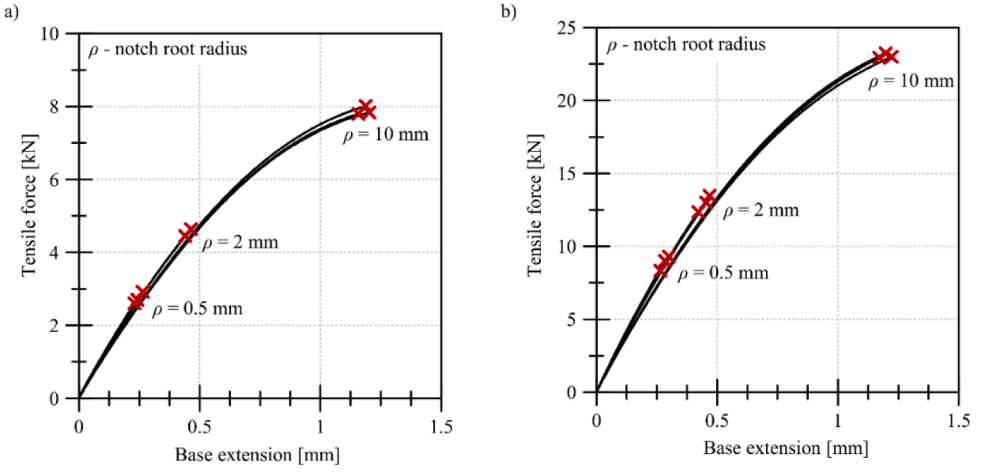


**Fig. 6.** Tensile curves for notched specimens with different root radii $\rho$, for nominal thickness $g$ equal to: a) 5 mm and b) 15 mm.

made were realised during tensile tests with torsion of cylindrical specimens. The paper [16] presents the results of the fracture tests on PMMA bars, weakened by ring notches. Experimental torsion-tension tests showed that the crack initiation angle measured from the symmetry plane of the specimen perpendicular to the direction of tension varies from 0° to 45°. The same type of failure was observed

**Table 2**
Critical tensile force values for notched specimens subjected to the uniaxial tension.

| Sample | $\rho$ | Nominal thickness | Maximum base extension | | Critical force value* | | Time to failure | |
|---|---|---|---|---|---|---|---|---|
| | [mm] | [mm] | [mm] | | [N] | | [s] | |
| | | | average | | average | | average | |
| 01–1-5 | 0.1 | 4.91 | 0.14 | | 1.68 | | 5.02 | |
| 01–2-5 | | 4.94 | 0.14 | | 1.67 | | 5.12 | |
| 01–3-5 | | 4.91 | 0.14 | **0.14** | 1.60 | **1.65** | 4.92 | **5.02** |
| 01–1-15 | | 15.04 | 0.15 | | 5.11 | | 6.22 | |
| 01–2-15 | | 14.38 | 0.15 | | 5.07 | | 6.12 | |
| 01–3-15 | | 15.03 | 0.16 | **0.15** | 5.27 | **5.15** | 6.42 | **6.25** |
| 05–1-5 | 0.5 | 4.92 | 0.23 | | 2.60 | | 8.02 | |
| 05–2-5 | | 4.93 | 0.24 | | 2.70 | | 8.42 | |
| 05–3-5 | | 4.92 | 0.26 | **0.24** | 2.92 | **2.74** | 9.23 | **8.56** |
| 05–1-15 | | 14.00 | 0.30 | | 9.31 | | 12.23 | |
| 05–2-15 | | 15.10 | 0.28 | | 9.00 | | 11.82 | |
| 05–3-15 | | 14.03 | 0.26 | **0.28** | 8.33 | **8.88** | 10.73 | **11.59** |
| 2–1-5 | 2 | 4.93 | 0.44 | | 4.45 | | 15.23 | |
| 2–2-5 | | 4.91 | 0.45 | | 4.55 | | 15.73 | |
| 2–3-5 | | 4.92 | 0.46 | **0.45** | 4.64 | **4.55** | 16.22 | **15.73** |
| 2–1-15 | | 13.94 | 0.47 | | 13.47 | | 19.23 | |
| 2–2-15 | | 15.27 | 0.45 | | 13.00 | | 18.74 | |
| 2–3-15 | | 15.51 | 0.42 | **0.45** | 12.35 | **12.94** | 17.73 | **18.57** |
| 10–1-5 | 10 | 4.91 | 1.19 | | 8.02 | | 38.06 | |
| 10–2-5 | | 4.91 | 1.16 | | 7.80 | | 37.55 | |
| 10–3-5 | | 4.91 | 1.21 | **1.19** | 7.84 | **7.88** | 38.45 | **38.02** |
| 10–1-15 | | 15.21 | 1.17 | | 23.00 | | 45.15 | |
| 10–2-15 | | 14.35 | 1.22 | | 22.93 | | 47.86 | |
| 10–3-15 | | 14.37 | 1.20 | **1.20** | 23.24 | **23.05** | 47.96 | **46.99** |

* Correction of force values: force read from the dynamometer · factor $k$, where $p$ = (nominal cross-sectional area) / (actual cross-sectional area of the specimen).

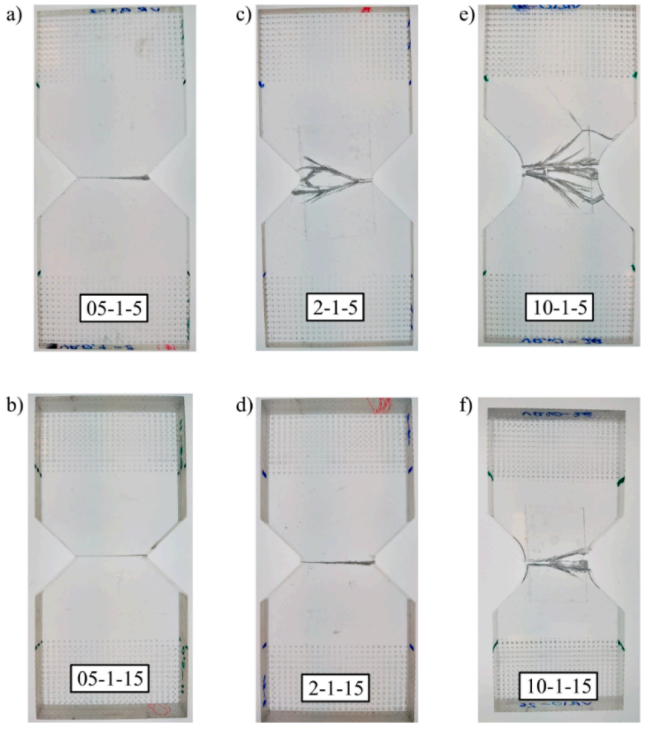


**Fig. 7.** Notched specimens with a root radius: $\rho = 0{,}5$ mm after tensile tests: a) $g = 5$ mm and b) $g = 15$ mm; $\rho = 2$ mm: c) $g = 5$ mm and a d) $g = 15$ mm; $\rho = 10$ mm: e) $g = 5$ mm and f) $g = 15$ mm.

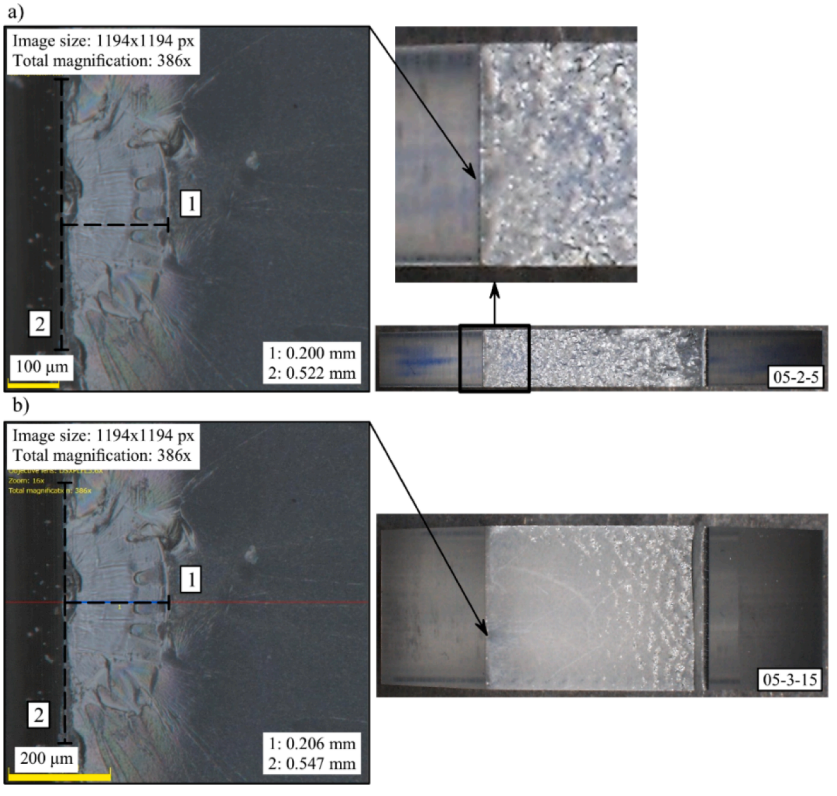


**Fig. 8.** Microscopic photograph of the fractures of tensile specimens weakened by V-notches with root radius $\rho = 0.5$ mm and nominal thickness: a) $g = 5$ mm, b) $g = 15$ mm.

in flat notched specimens, which were subjected to tensile tests using a special fixture. The first such solution was proposed in the work by Ayatollahi et al. [17].

A special set of grips is presented that makes it possible to realise in flat specimens weakened by a crack, pure states: opening and tearing, as well as intermediate configurations. Critical load values were obtained for PMMA 8-mm-thick specimens and used to calculate critical stress intensity factors. The crack initiation angles were determined from photos of the tested elements. Tests were repeated for specimens made of polystyrene (GPPS) [18]. The effect of specimen thickness and strain rate was considered in the studies described in the paper [19]. Tests showed changes in the material characteristics, from typically linear to strongly nonlinear, as the strain rate decreased. The effect of sample thickness became more pronounced the longer the process lasted. Studies of fracture processes in a complex configuration (mixed-mode I + III) using the above stand continued for other types of notches: [20,21,22,23]. The most popular brittle fracture criteria, i.e. the averaged stress criterion and the maximum tangential stress criterion, were positively verified.

Flat notched specimens made of plastic, repeatedly tested under compression [24–35]. The aforementioned papers describe the results of fracture tests for both pure notch opening and shearing, as well as their co-occurrence. The paper [33] not only estimated the critical values of the compressive force, but also indicated the different types of cracks that occurred. The work continued with the consideration of different loading speeds of a flat specimen [36].

The multitude of ongoing studies confirms that the issue of fracture of notched specimens made of plastics is still not fully described. Despite the many works on the fracture of components during notch opening, each successive experiment reveals new and interesting aspects of this phenomenon. So, in the present work, the focus was on expanding the tensile experiment described in the paper by Bura and Seweryn [6] to include flat specimens weakened by V-notches, also taking into account elements made of thin plates. The next step was to conduct torsion tests on the elements in the same shape. In the tests, the principle of maintaining a constant average strain rate was adopted, regardless of the loading method. This assumption is intended to eliminate the strong influence of strain rate on the results obtained [36]. With this approach, the description of the material in both loading cases will be possible using material constants with the same values of Young's modulus. Developing the fracture results separately for both states will enable the proper realisation of fracture studies of flat notched elements operating under complex states, i.e. torsion with tension.

## 2. Material and specimens

Polymethyl methacrylate (PMMA) is a thermoplastic polymer. Its popularity is growing mainly due to its fairly low price and good mechanical and optical properties. The plastic is used in many industries, such as biomedicine (as a component of bone cements, dental

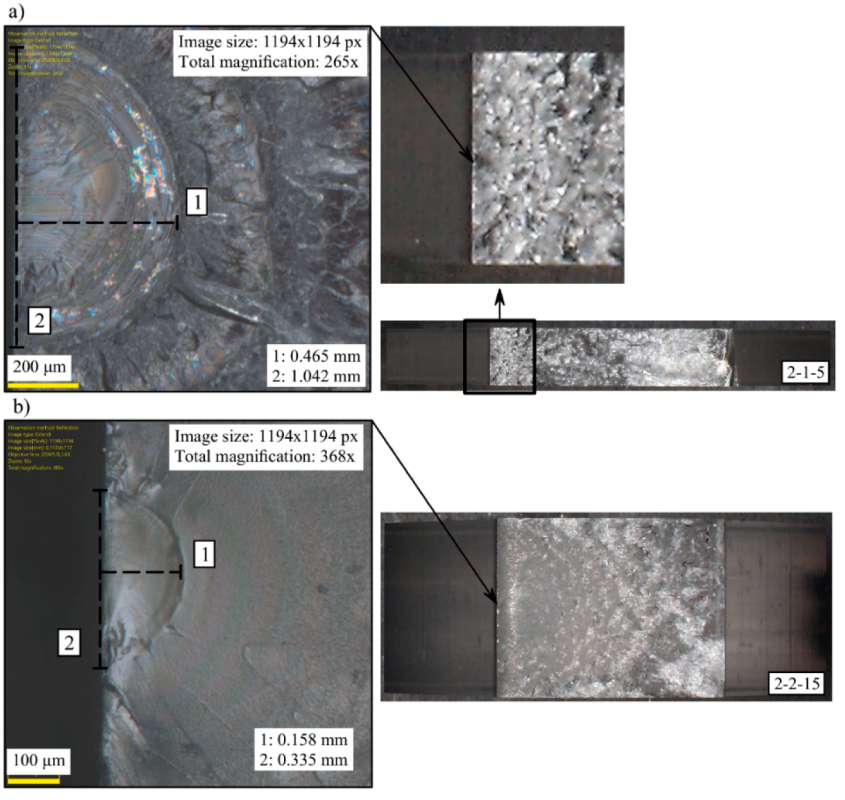


**Fig. 9.** Microscopic photograph of the fractures of tensile specimens weakened by V-notches with root radius $\rho = 2$ mm and nominal thickness: a) $g = 5$ mm, b) $g = 15$ mm.

prostheses due to its high bio tolerance), electrical engineering (LCD monitors), optics (lenses), as well as nanotechnology, automotive, transportation or architecture [37,38]. Among the most important properties of polymethylmethacrylate are its transparency and colourlessness. Pure polymethylmethacrylate is suitable for moulding by all thermal methods. The material is fully recyclable [39–41]. The plastic used in the study is specified by the trade name PLEXIGLAS®GS (Röhm GmbH). It was obtained in the form of cast sheets with nominal thicknesses of 5 and 15 mm. In order to determine the actual characteristics of the tested material (Table 1, Fig. 2), "paddle" type specimens (Fig. 1) were subjected to uniaxial tensile tests.

The shapes and dimensions of the specimens used are shown in Fig. 3. In order to study the effect of the size of the notch root radius on the fracture process, specimens were made with V-notches with an opening angle of 90° and radii of 0.5 mm; 2 mm and 10 mm. The parts were made in two thickness variants $g = 5$ and 15 mm (nominal thicknesses of the material sheet).

## 3. Research procedure

Strength tests were carried out using a dynamic biaxial testing machine, MTS 809.10, with an operating range of ± 100 kN for axial loads and ± 1100 Nm for torsional torque. The grips are equipped with self-clamping knurled jaws to prevent uncontrolled movement of the test pieces. Tests were conducted under controlled movement of the machine's chucks. The test stand is shown in Fig. 4 (configuration for tensile tests) and Fig. 5 (configuration for torsion tests). An important stage of testing was to indicate the moment and location of crack initiation, as well as to observe its propagation. For this purpose, a system of two monochrome cameras was used: PHANTOM v1610 and PHANTOM v2210, which are used to capture images at high speeds of up to one million frames per second. Depending on the type of load used, one or two cameras were employed.

### *3.1. Experimental results of notched element fracture in uniaxial tensile test*

Uniaxial tensile tests of notched specimens were carried out under controlled displacement conditions, which were set at a speed of 0.04 mm/s on a specimen base equal to 50 mm (averaged strain rate of about 0.0008 s-1). An axial extensometer measured the elongation of the specimen at a gauge base equal to 30 mm. Each element was loaded until failure. The entire process was monitored using a PHANTOM v2210 camera, which recorded the deformation process in the area of the measurement base from the front of the specimen (image resolution − 256 × 144 pixels; recording speed − 310,000 frames per second with an exposure time of 3.23 µs).

As a result of the above, the tensile curves shown in Fig. 6 were obtained. The data in the form of the maximum elongation of the

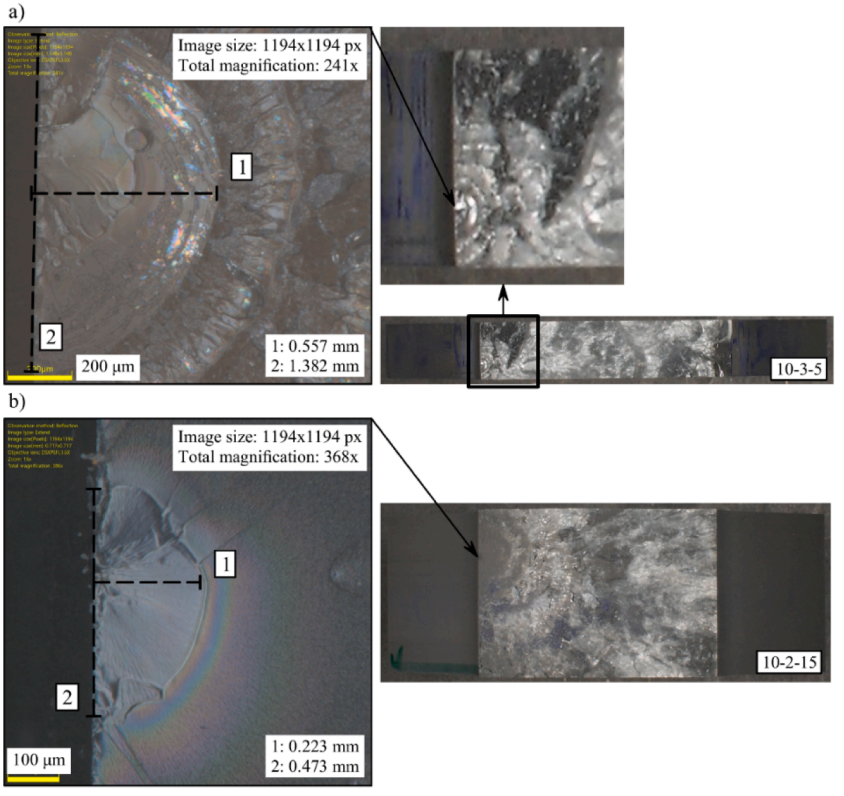


**Fig. 10.** Microscopic photograph of the fractures of tensile specimens weakened by V-notches with root radius $\rho = 10$ mm and nominal thickness: a) $g = 5$ mm, b) $g = 15$ mm.

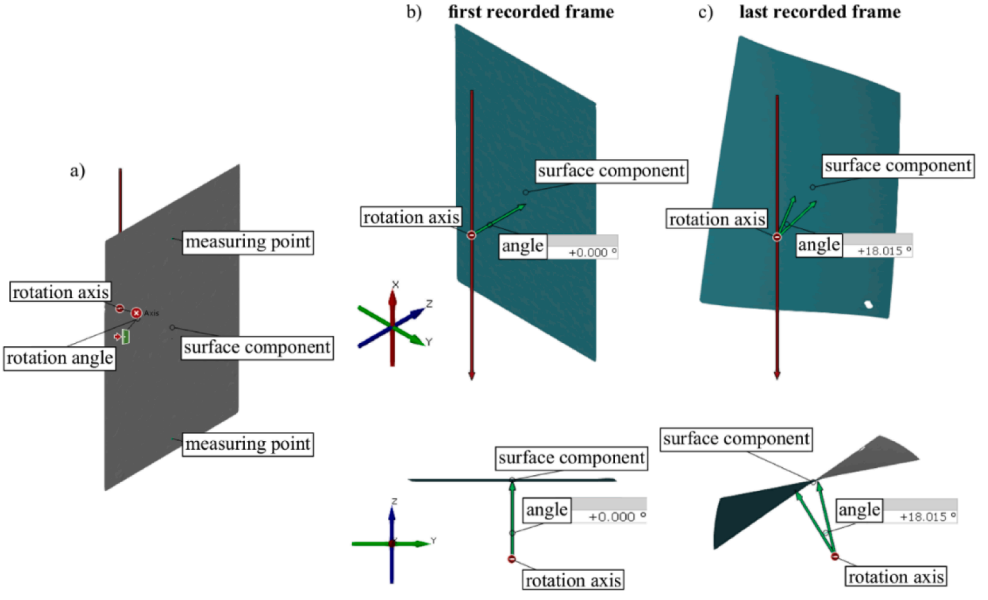


**Fig. 11.** Torsion angle measurement methodology using the ARAMIS 3D 4 M system: a) how to generate the rotation axis and b), c) how to measure the torsion angle.

measurement base, the critical value of the tensile force and the time to failure are summarised in Table 2. Analysing the nature of the tensile curves, it should be noted that as the notch root radius increases, a more pronounced non-linearity in the dependence of the force on the displacement of the gauge base is observed. In the case of specimens with notches with a radius of $\rho = 0.5$ mm, failure

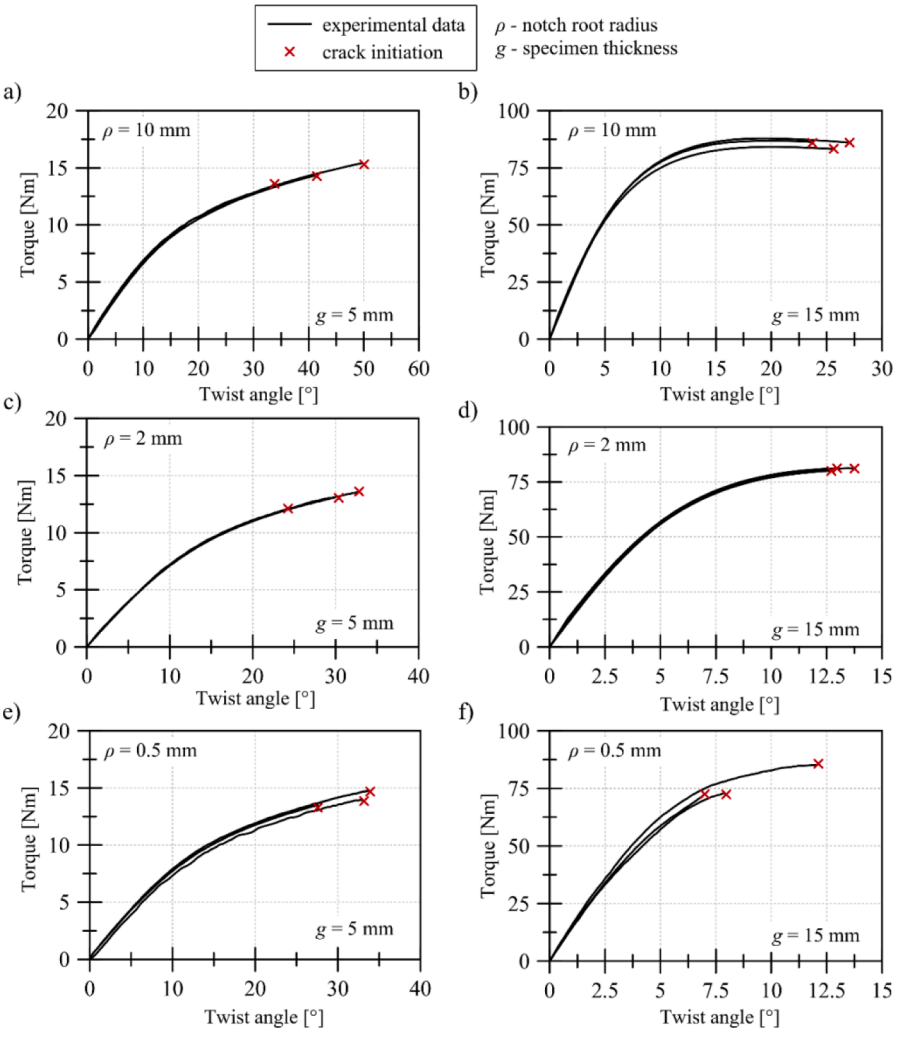


**Fig. 12.** Torsion curves for specimens weakened by notches of radius: a) b) $\rho = 10$ mm, c) d) $\rho = 2$ mm and e) f) $\rho = 0.5$ mm.

occurred in the near linear range, while the elongation of the gauge base did not exceed 0.3 mm. Tensile plots for specimens with the largest notch radius, i.e. $\rho = 10$ mm, are characterised by pronounced nonlinearity and an almost eight fold increase in gauge base elongation at about 1.2 mm. Specimens weakened by notches of the same root radius, but made from sheets of different thicknesses failed at similar levels of measuring base elongation.

Crack initiation always appeared near the bottom of the notch (once left once right). In all types of specimens, the crack initiation angle was found to be close to 0°, i.e. the crack initiated in the plane of symmetry of the specimen normal to the direction of loading. The specimens after the tests are shown in Fig. 7. The larger the radius of the notch tip rounding, the cracks cover a larger area of the specimen. As the radius $\rho$ increases, the time to the appearance of the first branches decreases and the total number of branches increases, resulting in a greater increase in new areas. The thicker the specimen, the less extensive the observed area of destruction (from the front of the specimen). For thicker elements, a greater amount of energy is lost to crack formation at the cross-section of the specimen; hence, a smaller number of branches is observed than for thinner specimens. This is best illustrated by images of elements weakened by notches with a notch tip rounding radius of $\rho = 2$ mm (Fig. 7).

An important element for describing the fracture phenomenon is the evaluation of the crack development surface. In the literature, one can find studies that evaluate the topography of cracks using, for example, a confocal measurement system [42]. Fractal analysis [43] of fractures can be another step to better understand the genesis of the fracture in flat notched specimens. In the present discussion, a basic assessment of the crack development surface was carried out. Using an OLYMPUS DSX1100 optical microscope, an analysis of the surface of the breakthrough near the bottom of the notch was carried out, which made it possible to determine the location of the crack initiation site. Figs. 8-10 show the fracture surfaces and the characteristic locations at the notch bottom. The crack initiation site was visible to the naked eye as a small smooth surface lying near the notch bottom. Magnification images showed that the crack initiation site had a semi-ellipsoid shape. For thinner specimens, this characteristic surface increases in area as the radius $\rho$ increases. The estimated averaged surface areas are 0.485 mm$^2$; 0.796 mm$^2$ and 0.973 mm$^2$, respectively, for a radius $\rho$ of 0.5, 2 and

**Table 3**
Critical values of torque and torsion angle for notched specimens subjected to the torsion.

| Sample | $\rho$ | Nominal thickness | Maximum torque | | Critical value of torsional moment | | Maximum value of torsional moment* | |
|---|---|---|---|---|---|---|---|---|
| | [mm] | [mm] | [°] | | [Nm] | | [Nm] | |
| | | | average | | average | | average | |
| S 05–1-5 | 0.5 | 4.92 | 33.17 | | 13.85 | | 13.85 | |
| S 05–2-5 | | 4.93 | 33.91 | | 14.68 | | 14.68 | |
| S 05–2-5 | | 4.92 | 27.58 | **31.55** | 13.28 | **13.94** | 13.28 | **13.94** |
| S 05–1-15 | | 14.66 | 12.12 | | 85.73 | | 85.73 | |
| S 05–2-15 | | 14.39 | 7.00 | | 72.52 | | 72.52 | |
| S 05–3-15 | | 14.19 | 7.97 | **9.03** | 72.38 | **76.88** | 72.38 | **76.88** |
| S 2–1-5 | 2 | 4.92 | 24.26 | | 12.11 | | 12.11 | |
| S 2–2-5 | | 4.92 | 30.39 | | 13.04 | | 13.04 | |
| S 2–3-5 | | 4.92 | 32.84 | **29.16** | 13.61 | **12.92** | 13.61 | **12.92** |
| S 2–1-15 | | 14.20 | 12.71 | | 80.03 | | 80.03 | |
| S 2–2-15 | | 14.26 | 12.96 | | 81.18 | | 81.18 | |
| S 2–3-15 | | 14.07 | 13.75 | **13.14** | 81.08 | **80.76** | 81.08 | **80.76** |
| S 10–1-5 | 10 | 4.92 | 41.47 | | 14.26 | | 14.26 | |
| S 10–2-5 | | 4.92 | 33.83 | | 13.59 | | 13.59 | |
| S 10–3-5 | | 4.92 | 50.06 | **41.79** | 15.30 | **14.38** | 15.30 | **14.38** |
| S 10–1-15 | | 14.70 | 23.71 | | 85.92 | | 86.83 | |
| S 10–2-15 | | 14.69 | 27.06 | | 86.03 | | 87.90 | |
| S 10–3-15 | | 14.49 | 25.64 | **25.48** | 83.32 | **85.09*** | 84.20 | **86.31*** |

* different from the critical value.

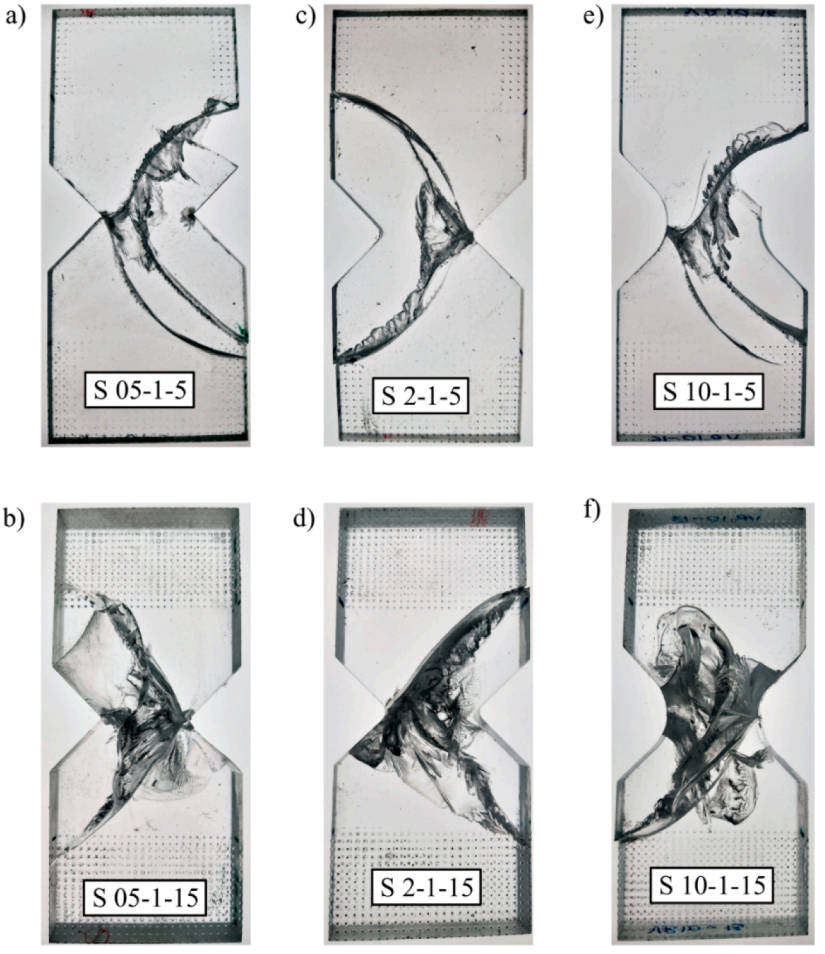


**Fig. 13.** Notched specimens with a root radius: $\rho = 0.5$ mm after torsion tests: a) $g = 5$ mm and b) $g = 15$ mm; $\rho = 2$ mm: c) $g = 5$ mm and a d) $g = 15$ mm; $\rho = 10$ mm: e) $g = 5$ mm and f) $g = 15$ mm.

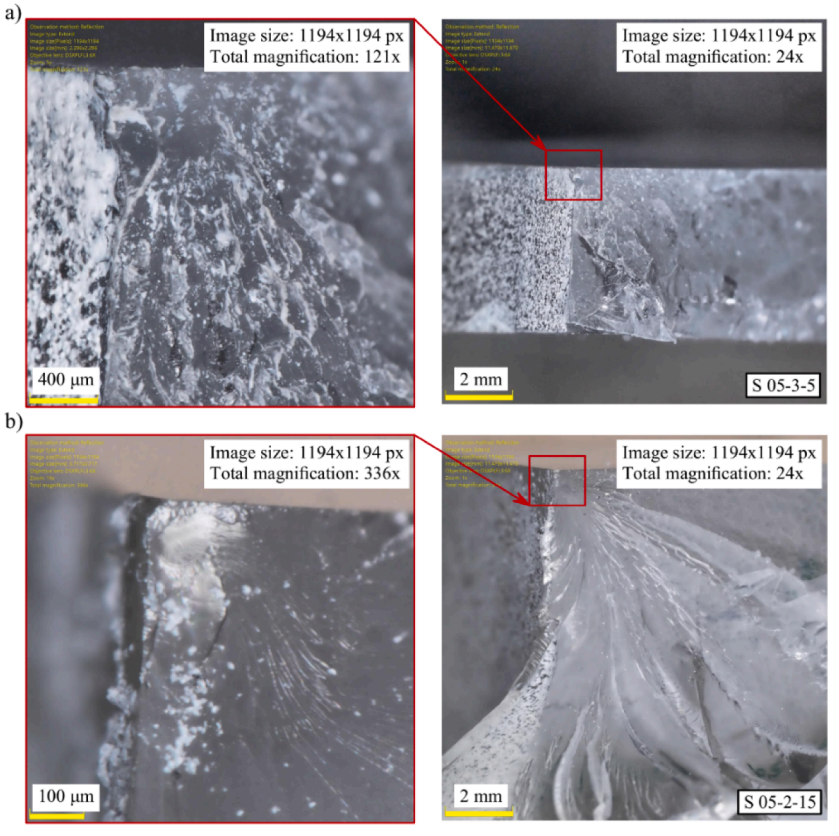


**Fig. 14.** Microscopic images of fracture surface of specimens subjected to torsion, weakened by V-notches with root radius $\rho = 0.5$ mm and nominal thickness: a) $g = 5$ mm, b) $g = 15$ mm.

10 mm. In the case of thick specimens, no such tendency was noticed, and the area of this area remains at about 0.243 mm$^2$. From this area, the fracture process begins and then propagates deep into the specimen, as evidenced by the bars seen in the images. Crack usually initiated at the notch bottom. The situation was different only in the case of specimens with the notch with the largest root radius. The crack initiated from around the symmetry plane of the specimen, and only in isolated cases from the lateral surface of the specimen. In this case, too, the discrepancies in the results may be due to material defects, but also to slight differences in the thickness of the component in question (the samples were made from cast plates). The finite (albeit very small) dimension of the crack initiation surface to some extent justifies a non-local approach [44,45]. This is based on the assumption that the crack occurs simultaneously in this area. However, it could also be an indication that cracking starts at a certain point close to the free surface and then propagates toward it. The same applies to the propagation of an already existing crack. Stripes on the fracture surface can indicate that the crack propagation is a discrete process (takes place "in steps"): from a certain point in front of the crack tip toward the crack tip.

### 3.2. *Experimental results of notched element fracture in the torsion test*

The problem of measuring the torsion angle was solved using the method of digital image correlation - ARAMIS 3D 4 M vision system (Fig. 5), which is used for non-contact displacement measurements by means of digital image correlation. A measurement plane was generated in the measurement base of the sample. The next step was to create the axis of rotation, which was always fixed at the actual centre of gravity of the specimen in question (Fig. 11a). The torsion angle measured on the measurement plane was obtained as the difference of the torsion angles determined for two measurement points relative to the established axis of rotation (Fig. 11a). The points were chosen according to the dimensions of the measuring base, i.e. 25 mm and 30 mm, for smooth and notched specimens, respectively. The measurement was always made at the axis that is the intersection of the symmetry planes of the specimen. Fig. 11b, c shows how the twist angle was measured for the first and last recorded frames.

Experimental studies of fracture during torsion began by determining the appropriate angular displacement setting speed. It was assumed that the averaged strain rate during pure tension and torsion should be as close as possible, since the material is highly sensitive to changes in this magnitude. Keeping the averaged strain rate constant during each type of loading will make it possible, at a later stage of numerical calculations, to use the same strengthening curve to describe the material. To this end, a series of torsion tests were carried out on smooth specimens at different angular displacement speeds of the measuring base. Linear sections of torsion were analysed, from which the value of Kirchhoff's modulus was determined. The appropriate angular displacement velocity of the

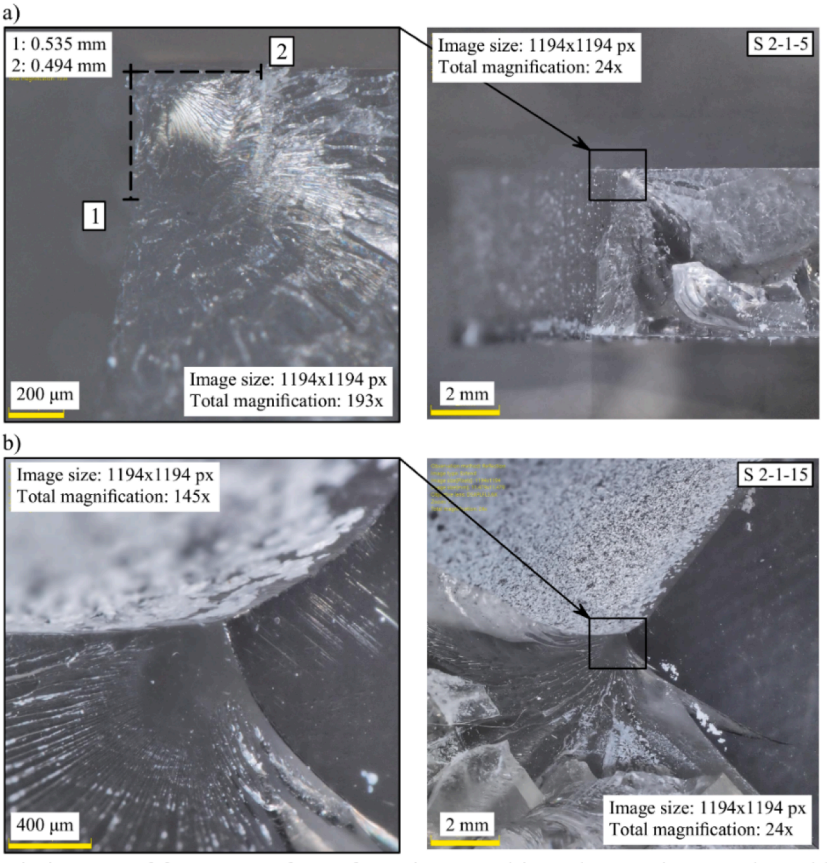


**Fig. 15.** Microscopic images of fracture surface of specimens subjected to torsion, weakened by V-notches with root radius $\rho = 2$ mm and nominal thickness: a) $g = 5$ mm, b) $g = 15$ mm.

measurement base was taken to be the one for which the value of the modulus resulted from the relation: $G = E/2(1 + \nu)$(Young's modulus and Poisson's ratio values were determined in tensile tests). The strain rate is affected not only by the speed of the displacement or torsion angle setting, but also by the thickness of the specimen. The velocity of angular displacement of the measurement base for specimens with a nominal thickness of $g = 15$ mm was assumed to be$\dot{\phi} = 0{,}09°/s$. And for specimens with a nominal thickness of $g = 5$ mm, $\dot{\phi} = 0{,}15°/s$. was considered the optimal speed. As a result of the above measures on notched specimens, the torsion curves shown in Fig. 12 a-f, were obtained. The plots indicate the moment of crack initiation. The data in the form of the maximum torsion angle of the gauge base and the critical value of the torsional moment are summarised in Table 3.

The smaller the notch root radius, the smaller the critical value of the twist angle. For specimens with a nominal thickness of $g = 15$ mm, it was on average: 25°, 13° and 9° (Fig. 12d-f) for a radius $\rho$ of 10, 2 and 0.5 mm, respectively. Similar trends were observed for specimens with a thickness of $g = 5$ mm (Fig. 12a-c), but very similar values of this angle were obtained for the two smallest radii. The notch root radius $\rho$ had a strong influence on the value of the torsion angle at which crack initiation occurs, but the critical value of the torsional moment appears to be independent of it, since all types of specimens had similar cross-sectional areas at the base of the specimen. For specimens with a thickness of $g = 5$ mm (Fig. 12a-c), crack initiation occurred when the torsional moment reached a value of about $13.5 \pm 0.5$ Nm. For specimens with a thickness of $g = 15$ mm (Fig. 12d-f), it was about $80 \pm 5$ Nm. In the latter case, the tendency for the critical value of the torsional moment to increase with an increase in the value of the notch root radius was somewhat more pronounced. However, these are small increments of about 6%.

A strong influence of the specimen thickness on the value of the maximum torsion angle was also observed; the thinner the sample the more prone to torsion. For the different types of notches, about twice the maximum torsion angle was observed for samples with a nominal thickness of $g = 5$ mm compared to samples with a nominal thickness of $g = 15$ mm. In all cases, the dependence of the torsional moment on the torsion angle had a nonlinear character. Special attention should be paid to specimens with thickness $g = 15$ mm and radius $\rho = 10$ mm (Fig. 12d). In this case, the maximum value of the torsional moment was not equal to the critical value. After reaching the extreme, the value of the torque began to decrease slightly until failure. In the fracture model of plastics (PMMA), it is necessary to take into account the state of stress in the elements; in particular, the place of occurrence and the value of maximum normal stresses, but also the values of plastic deformation, which cause not only a change in the shape of the element, but also a decrease in the value of destructive stresses for the material (hence the observed decrease in the value of torsional moment in its

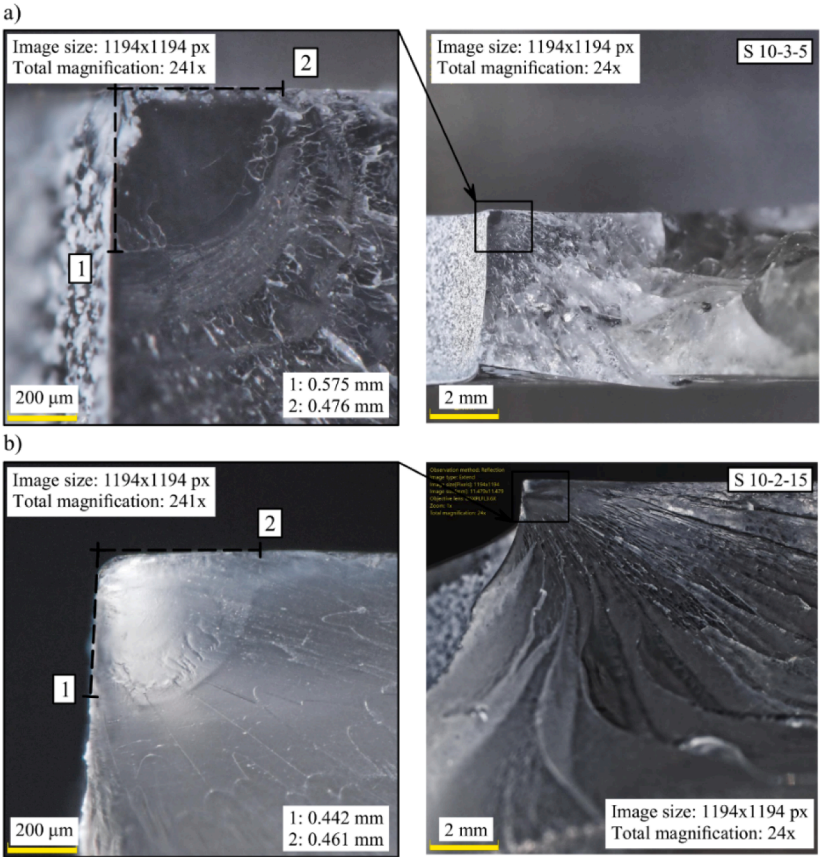


**Fig. 16.** Microscopic images of fracture surface of specimens subjected to torsion, weakened by V-notches with root radius $\rho = 10$ mm and nominal thickness: a) $g = 5$ mm, b) $g = 15$ mm.

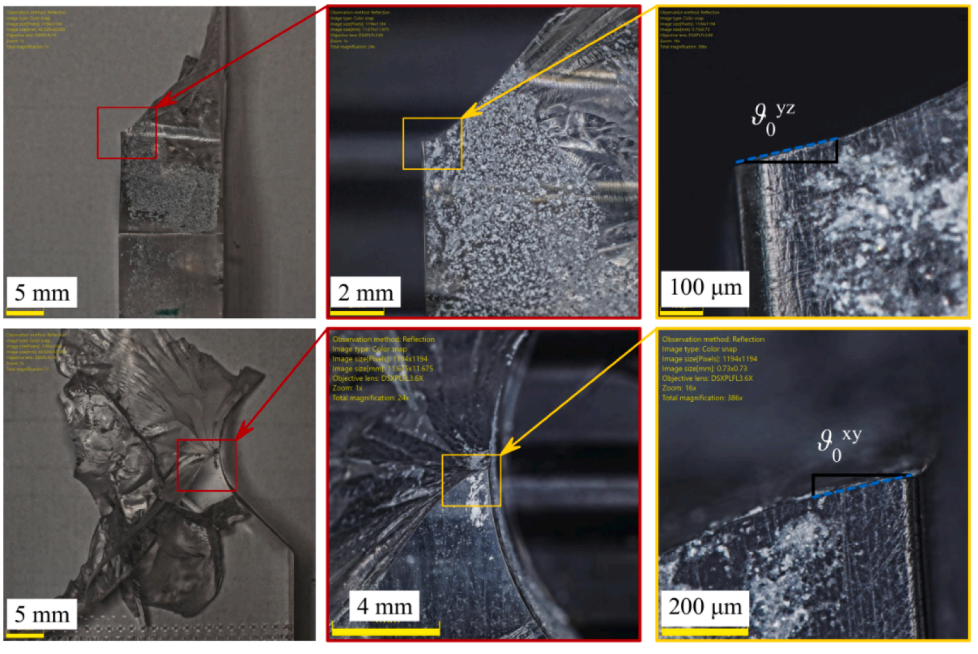


**Fig. 17.** Microscopic measurements of the angular position of the edge of the crack initiation surface.

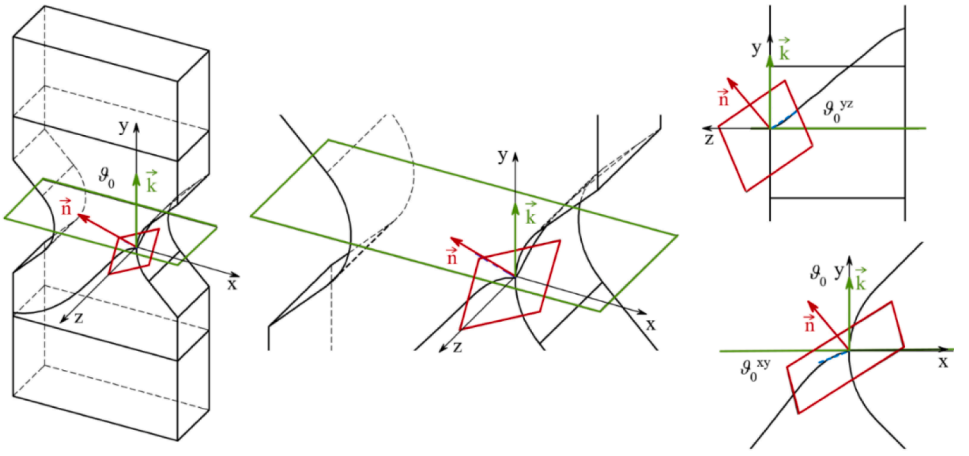


**Fig. 18.** The relative position of the fracture plane during pure torsion with respect to the horizontal symmetry plane of the specimen (plane of crack initiation during pure tension).

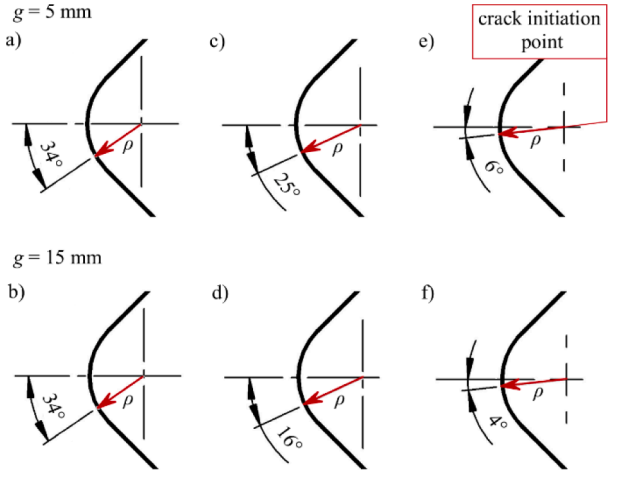


**Fig. 19.** Location of the crack initiation point on the notch bottom edge, the notch root radius $\rho$ equal to: a) b) 0.5 mm; c) d) 2 mm and e) f) 10 mm.

dependence on the torsion angle (in the final range) for some twisted samples. It follows that fracture criteria should be formulated in a manner similar to fracture criteria for metal alloys, such as aluminium alloy [46,47]. The specimens after the tests are shown in Fig. 13. A completely different character of destruction than in the case of tension was observed. Destruction covers virtually the entire area of the specimen's measuring base. In the case of elements with a nominal thickness of $g = 5$ mm, it can be seen that the crack always initiated from the region of the notch bottom and propagated by branching out just after initiation. In notched specimens with a radius of $\rho = 0.5$ mm, bifurcation took place almost, at the same place as initiation, and the propagating crack fronts circle a semicircle with a radius of about 25 mm, the centre of which coincides with the notch symmetry axis and the outer edge of the specimen (Fig. 13a). The larger the notch root radius, the branching of the main crack occurred later, and the centre of the semicircle that the crack circled moved outside the outline of the specimen. For specimens with a nominal thickness of $g = 15$ mm, the areas of failure for all cases of radius $\rho$, appear to be very similar.

The locations of crack initiation were characterised on the basis of microscopic images of fracture surfaces. Determination of critical points was more difficult than in tensile specimens because of the change in the angular position of the failure surface relative to the symmetry plane of the specimen. The indicated characteristic dimensions of the surfaces from which the fracture initiated should be considered approximate due to the lack of a uniform reference point used in the observations. In the case of specimens with a notch radius of $\rho = 0.5$ mm, it was difficult, and sometimes even impossible, to determine the location of crack initiation on the basis of fracture surface analysis because of the extensive deterioration of the specimens.

Fig. 14 shows close-ups of the established points from which the crack initiated. They were located at the edge of the specimen near the notch bottom. The fracture surfaces clearly indicate the direction of damage development. For the other types of specimens (Figs. 15 and 16), the crack initiation points were visible on the fracture surfaces as a small smooth area lying near the notch bottom. Magnification images showed that the crack initiation site had the shape of a quarter ellipse, with its centre located at the specimen

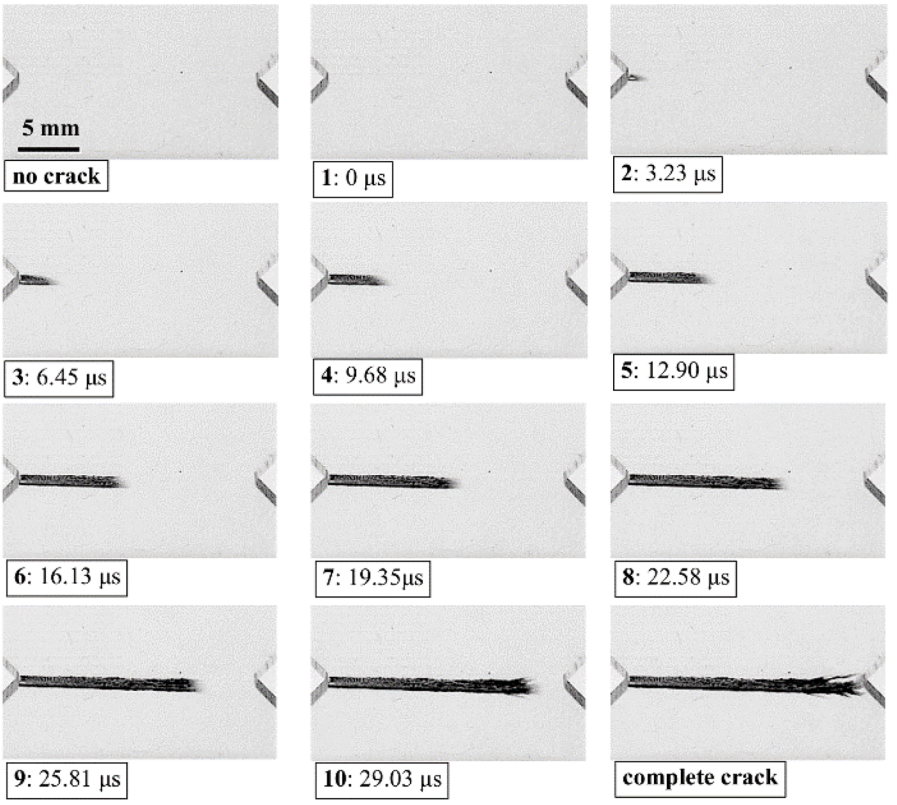


**Fig. 20.** Crack propagation during tension in a notched specimen (0.5–1-5) with notch root radius $\rho = 0.5$ mm and nominal thickness $g = 5$ mm.

edge. The estimated averaged surface areas for specimens with a nominal thickness of $g = 5$ mm were: 0.208 mm$^2$ and 0.149 mm$^2$, respectively, for a radius $\rho$ of 2 and 10 mm. For thicker samples ($g = 15$ mm), the area of this surface was about 0.162 mm$^2$ and 0.142 mm$^2$, respectively. All these values are close to $g = 5$ mm each other. It can be concluded that there is no effect of the notch root radius, as well as the thickness of the flat specimen, on the location of the crack initiation site during torsion tests.

The crack initiation angle $\vartheta_0$ was measured on the basis of tested specimens photographs. The reference element was the horizontal symmetry plane of the specimen described by the normal vector $\bar{k}$, which is simultaneously the notch symmetry plane and the plane of crack initiation during pure tension. Appropriately oriented on the moving microscope table, the specimens were observed from two directions (Fig. 17), from the front and from the lateral surface, so as to identify the edges of the crack initiation surface – in reference to those surfaces indicated in Figs. 14–16.

Having the projections of the edges in question, their angular positions $\vartheta_0^{xy}$ and $\vartheta_0^{yz}$ were determined with respect to the axis of the coordinate system inscribed at their point of intersection (Fig. 18). The plane described by these edges can be considered, as the plane of crack initiation, and its inclination with respect to the horizontal symmetry plane of the specimen (the angle between the normal vectors of these planes) was taken as the angle of crack initiation. Different values of the crack initiation angle were obtained depending on the specimen thickness and the notch root radius. For specimens with radius $\rho = 2$ mm, the crack initiation angle $\vartheta_0$ was on average: 37° and 40°, while for $\rho = 10$ mm, $\vartheta_0$ equal to about 28° and 24° were recorded (for specimens with nominal thicknesses of 5 and 15 mm, respectively). It can be concluded that the larger the notch root radius, the smaller the crack initiation angle.

The location of the crack initiation point at the edge of the notch bottom was also indicated (Fig. 19). The angle formed by the radius associated with the averaged crack initiation point with the notch symmetry axis was measured. The destruction had its origin at the edge of the notch bottom, but not in its symmetry plane. For specimens with a thickness of $g = 5$ mm, the angle in question reaches values of about 34°, 25° and 6°, respectively, for a radius $\rho$ of: a) 0.5 mm, b) 2 mm and c) 10 mm. Thus, the smaller the notch root radius, the greater the value of the angle by which the crack initiation point rotates relative to the notch symmetry plane. The same relationships hold for specimens with a nominal thickness of $g = 15$ mm. An interesting case turns out to be specimens with notches with a radius of $\rho = 0.5$ mm, for which the same position of the crack initiation point was observed for both tested specimen thicknesses. In other elements, it was noted that the thicker the sample, the location of the initiation sites was closer to the symmetry plane of the sample. Since crack initiation results in a smooth free surface with a specific orientation, the fracture criterion should be related to the state of stress on the physical plane [44,48]. This orientation follows the direction of maximum normal stresses. Studies have not resolved what role cutting stresses play in the fracture process and whether they should be included in the fracture criteria.

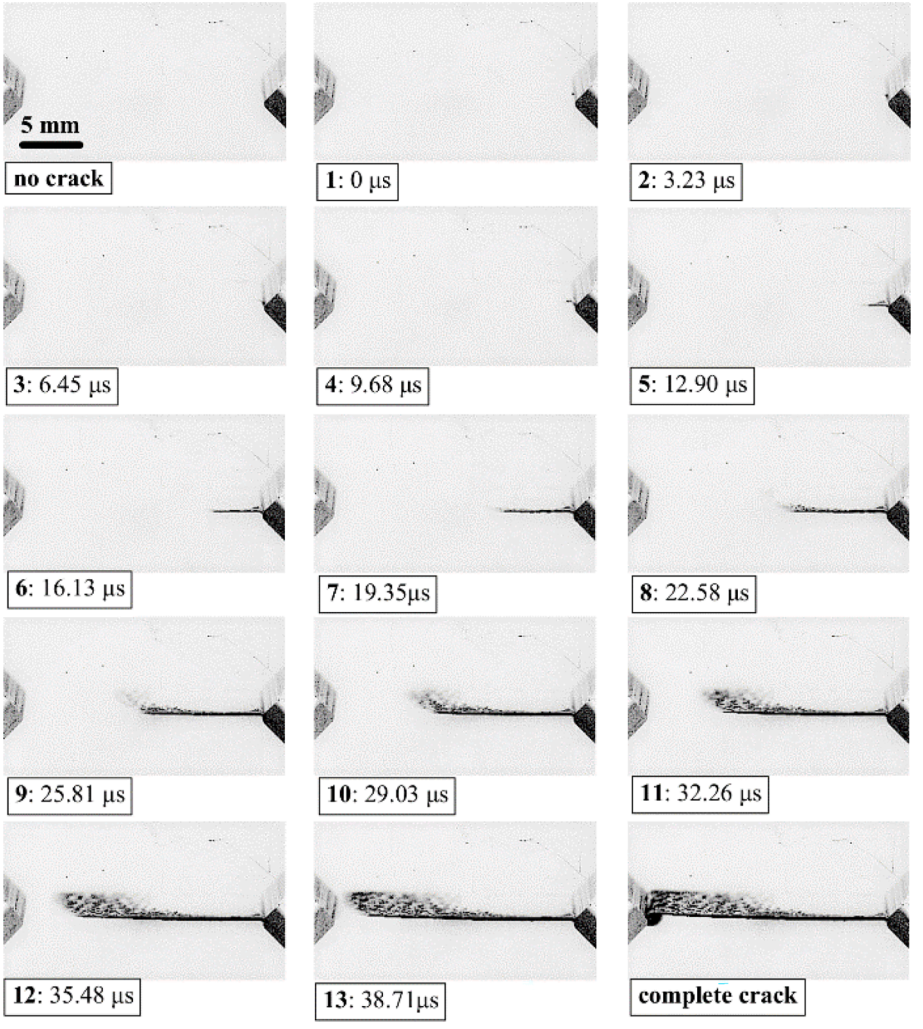


**Fig. 21.** Crack propagation during tension in a notched specimen (0.5–2-15) with notch root radius $\rho = 0.5$ mm and nominal thickness $g = 15$ mm.

## 4. Crack propagation during tension and torsion tests

The test stand was equipped with a camera system for taking high-speed images, primarily to determine the locations and moments of crack initiation. The recordings obtained also made it possible to trace the propagation process of these cracks. Monotonic tensile tests were recorded with a PHANTOM v2210 monochrome camera at 310 000 frames per second, so that each frame was recorded every 3.23 μs. In the case of torsion tests, due to the different recording speeds of the two cameras, the frequency of recording subsequent frames will be different depending on which camera managed to capture the moment of crack initiation and its subsequent development. Based on the methodology described in the paper [6], the velocities of crack front travel were estimated, and how the notch root radius and the specimen thickness affect the crack propagation velocity during uniaxial tension (the case of notch opening - mode I) was investigated. Each case was interpreted individually. Attempts at any automatic image analysis proved to carry a large computational error. The problems were mainly related to the lighting conditions of the elements, which were the same for all cases. Different runs of the fracture process caused the crack surfaces to absorb or reflect light in different ways. The frame on which the crack was clearly visible was taken as the beginning of the process, after which the position of the crack front was determined, and this operation was repeated on subsequent frames, omitting the one on which the crack reached the bottom of the opposite notch. The last frame was discarded due to the fact that the cracking may have ended before the camera recorded it. Hence, propagation velocities were determined excluding the first (no crack) and last frame (complete crack). Records of the crack propagation process for all samples are shown in Figs. 20–25. By far the longest crack propagated to the second notch bottom for the smallest notch root radius $\rho = 0.5$ mm. The average crack development time for this type of specimen is about 30 μs (for both thicknesses). A four-fold increase in the radius $\rho$ resulted in an acceleration of the process by about 20% (the average time was about 24 μs). For notched samples with a radius of $\rho = 10$ mm, the crack propagated for an average of about 21 μs. Estimating the total crack development time may carry some error, mainly because the first visible crack was recorded at different times in its development, so it seems more accurate to estimate

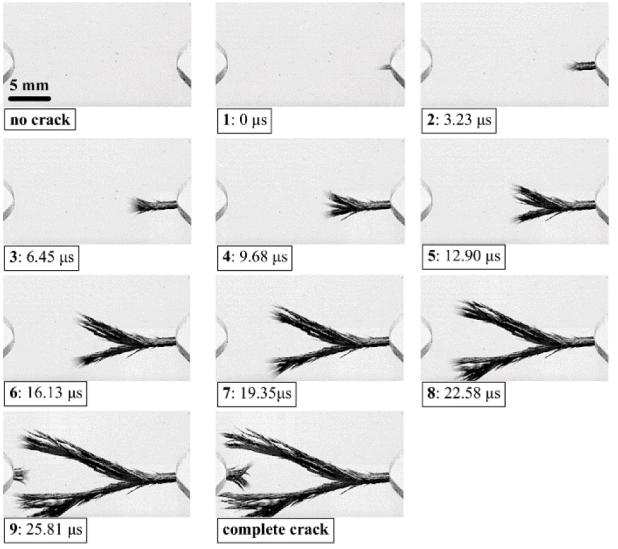


**Fig. 22.** Crack propagation during tension in a notched specimen (2–1-5) with notch root radius $\rho = 2$ mm and nominal thickness $g = 5$ mm.

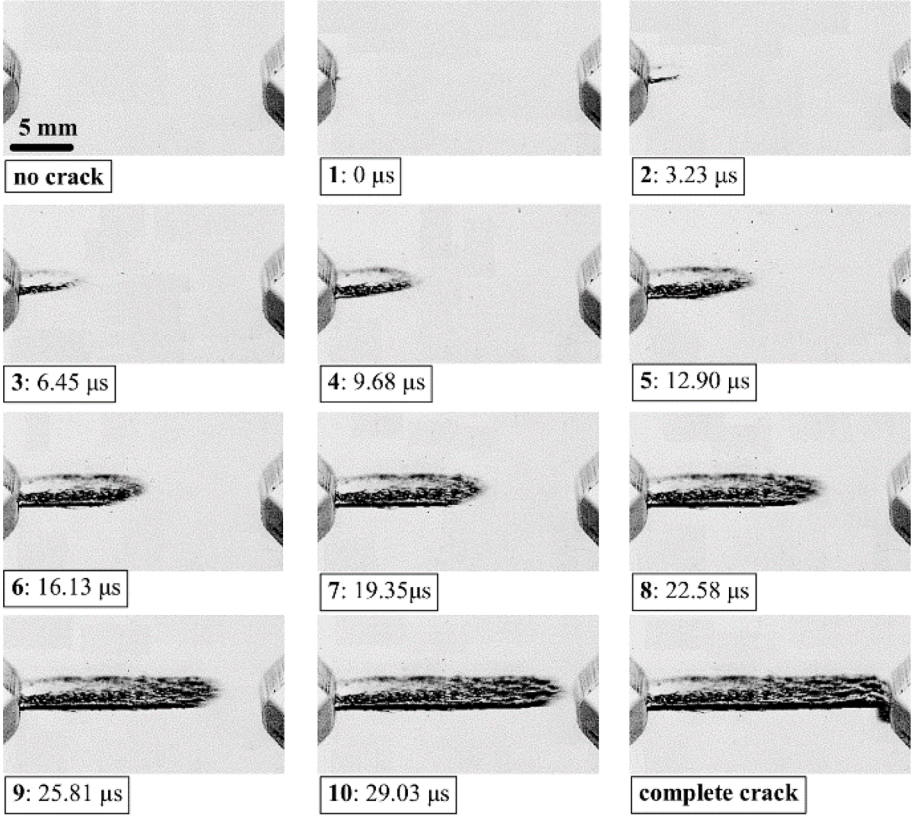


**Fig. 23.** Crack propagation during tension in a notched specimen (2–2-15) with notch root radius $\rho = 2$ mm and nominal thickness $g = 15$ mm.

the propagation speed. In this case, the tendency is again apparent that the larger the notch root radius, both the averaged crack development speed and the maximum values will be higher. For the case of $\rho = 0.5$ mm, the crack propagated with an average velocity of no more than 600 m/s, and the maximum values reached about 700 m/s. In notched specimens with the largest radius $\rho = 10$ mm, average values were recorded at levels far exceeding 700 m/s, with maximum values even reaching values above 1 000 m/s. The smaller the notch root, the higher was the strain energy of the specimen, accelerating the crack initiation. If the specimen failed at

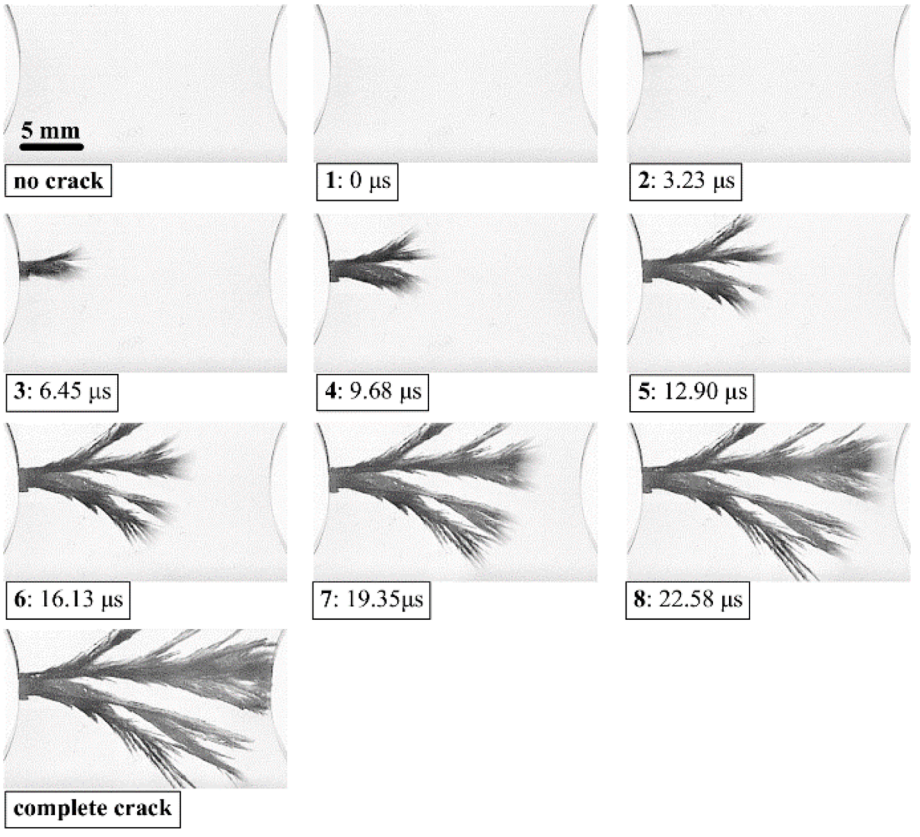


**Fig. 24.** Crack propagation during tension in a notched specimen (10–1-5) with notch root radius $\rho = 10$ mm and nominal thickness $g = 5$ mm.

smaller values of tensile force, less energy was released in the fracture process (relative to larger radii $\rho$), and the crack propagated more slowly.

The data also show that the thickness of the specimen significantly affects the crack propagation process. The values of averaged crack propagation velocities are generally higher for thinner specimens (nominal thickness $g = 5$ mm). The element thickness is crucial at the beginning of the process, since the crack initiated mainly from around the centre of the specimen thickness. Thus, the first stage of its development was not only about propagation toward the bottom of the opposite notch, but also about the direction along the specimen thickness. The thicker the specimen, the crack front reached lower velocities at the beginning of the process. The further the stage of crack development, the differences in its propagation speeds obtained for the same notches but different sample thicknesses turned out to be smaller.

Estimating the crack propagation velocity during torsion is not as obvious as in the case of uniaxial tensile testing, where the plane of failure coincided with the notch symmetry plane. The study presented in this paper is a starting point for work on a test stand and test methodology that will facilitate a realistic estimate of the speed at which crack propagation occurs during pure torsion tests. Selected moments of the deformation process of specimens with a nominal thickness of $g = 15$ mm, which enable verification of the previously described conclusions, are summarised below. Fig. 26 shows three frames for each specimen. The first - a frame preceding the visible crack initiation, the second - a frame close to the moment of crack initiation (the red arrow indicates the location of crack initiation), and the third - a frame obtained after a certain time. In general, similar choices were made for all recording speeds. Next to each of the images is the time of crack development, with the first frame where the crack was noticed, which is not always equal to its initiation, at beginning of this process.

In all cases, the crack initiates from the lateral edge of the notch bottom, but does not lie in its symmetry plane. At the time of critical loading, there are four critical points in the specimen where a crack can initiate. The parts underwent fracture, once in the left and once in the right notch, with one at its front and one at its back edge. The difficulty of comparing the crack size areas at a given point in time is ideally demonstrated by the compiled images for specimens with a nominal thickness of $g = 15$ mm. Depending on which point initiated the crack, the observer sees the fracture surface from a different angle. A full description of the crack development would, be possible with more cameras, observing the sample from each direction. Comparing the crack size (the occupied area of the frame) for similar time since crack initiation and for different specimens thicknesses, it can be said with certainty that in thinner specimens the crack propagates faster into the depth of the specimen. To further describe the nature of crack propagation during torsion, frame-by-frame processes are shown for selected samples of each type (Figs. 27–32).

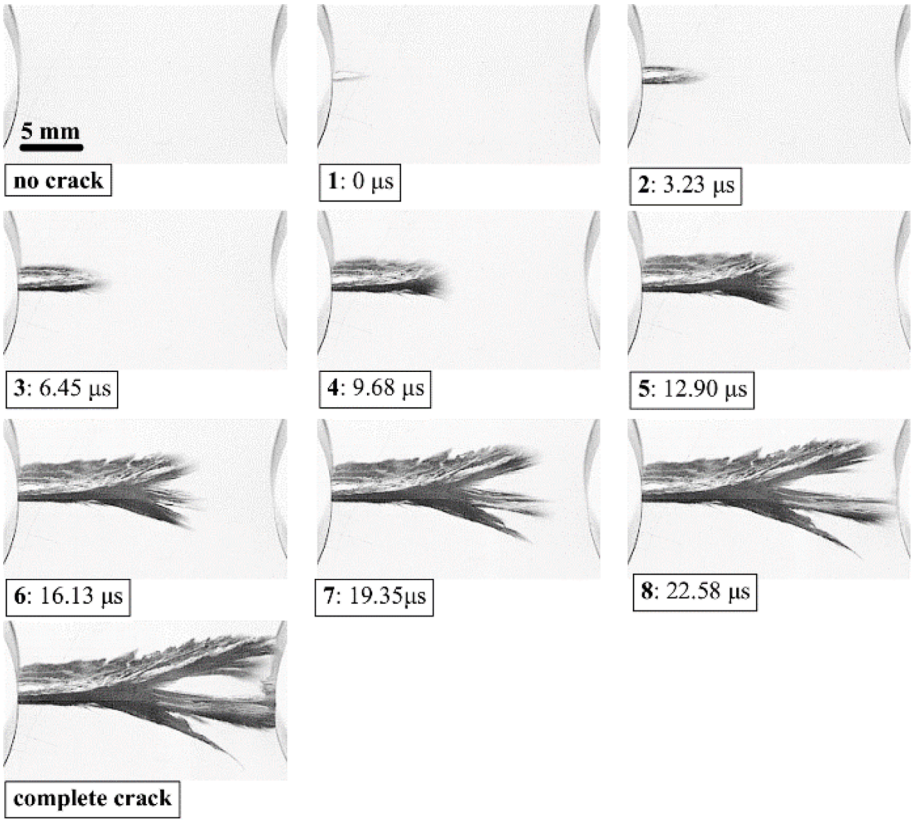


**Fig. 25.** Crack propagation during tension in a notched specimen (10–1-15) with notch root radius $\rho = 10$ mm and nominal thickness $g = 15$ mm.

Once again, it can be seen that for thinner specimens, the crack propagates much faster beyond the area observed by the cameras. In addition, the analysis is made more difficult by the much larger twist angle of the specimen. One can tentatively conclude that the greater the twist angle, the faster the cracks propagated. This is a similar trend to that of tensile tests, due to the higher potential energy of these specimens, which is released for the formation of new free surfaces.

## 5. Concluding remarks

The experimental results of the fracture of flat notched specimens under tensile or torsional loading presented in this paper provide insight into the fracture process and can be the basis for numerical modelling, as well as the formulation of an adequate fracture criterion. Analysis of these results leads to a number of conclusions, the most important of which will be presented below.

The fracture of notched parts made of plastics such as PMMA is a nonlinear phenomenon, which is particularly evident during the fracture of specimens subjected to torsion (strongly nonlinear dependence of the torsional moment on the torsion angle of the specimen). This indicates the existence of plastic deformation, which cannot be neglected during numerical simulation of the process of deformation and fracture of the material, especially in the case of larger notch root radii $\rho = 10$ mm. Linear fracture mechanics relations can only be used to estimate the critical load in the case of tensile elements with notches of very small notch root radius (or sharp). In all cases, the dependence of the torsional moment on the torsion angle had a nonlinear character. It should be noted that for $\rho = 10$ mm, the maximum value of the torsional moment (86.31 Nm) was not equal to the critical value (85.09 Nm).

In all cases the location of crack initiation was as a small smooth surface lying near the notch bottom. After the tensile tests the crack initiation site had a semi-ellipsoid shape located in the vicinity of the specimen thickness centre. After the torsion tests it had the shape of a quarter ellipse, with its centre located at the specimen edge. It can be concluded that there is no effect of the notch root radius, as well as the thickness of the flat specimen, on the location of the crack initiation site during torsion tests. Only the type of load affects the location of the crack initiation site.

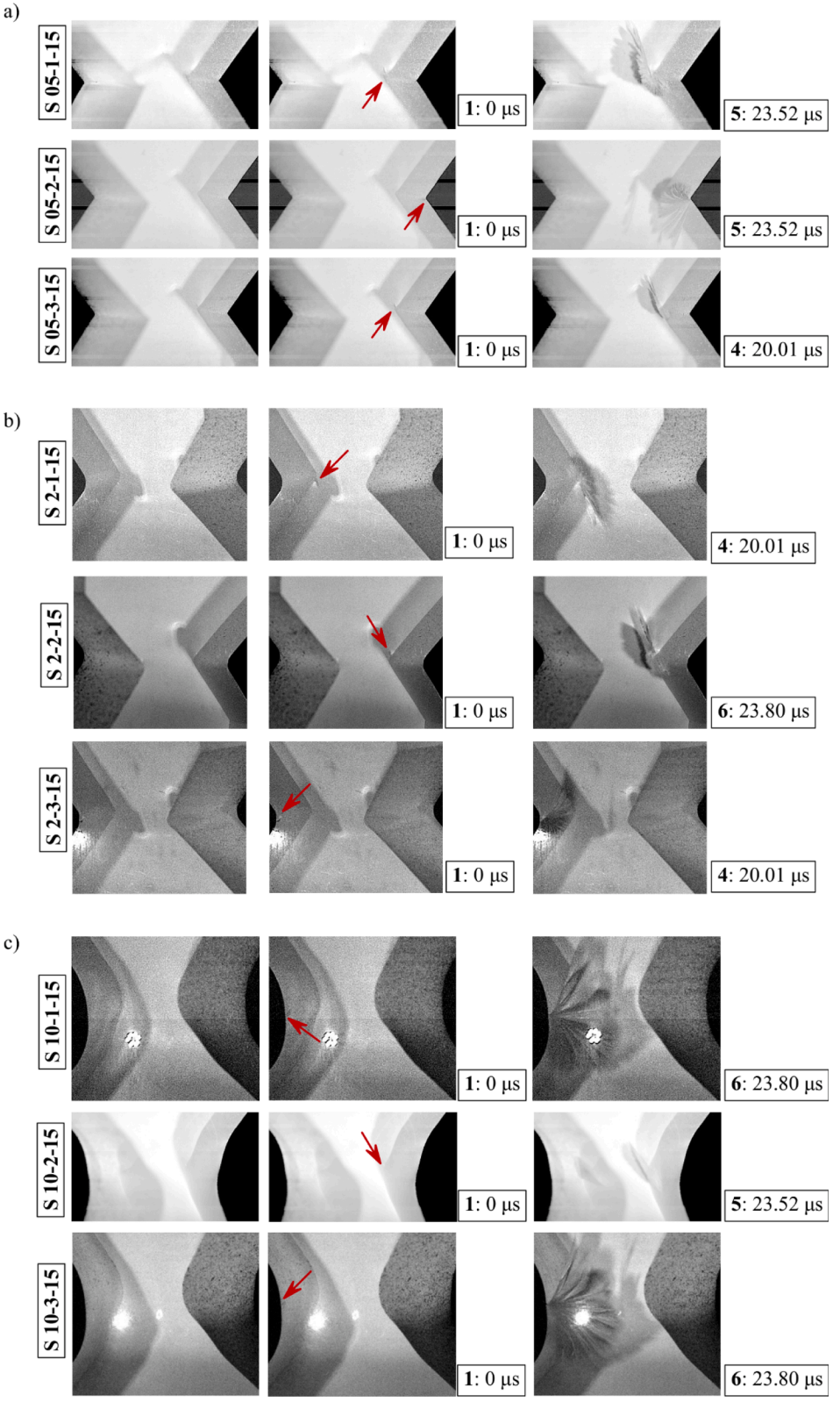


**Fig. 26.** The location of crack initiation and the nature of its propagation during torsion at the selected time step for notched specimens with: a) $\rho =$ 0.5 mm, b) $\rho = 2$ mm and c) $\rho = 10$ mm.

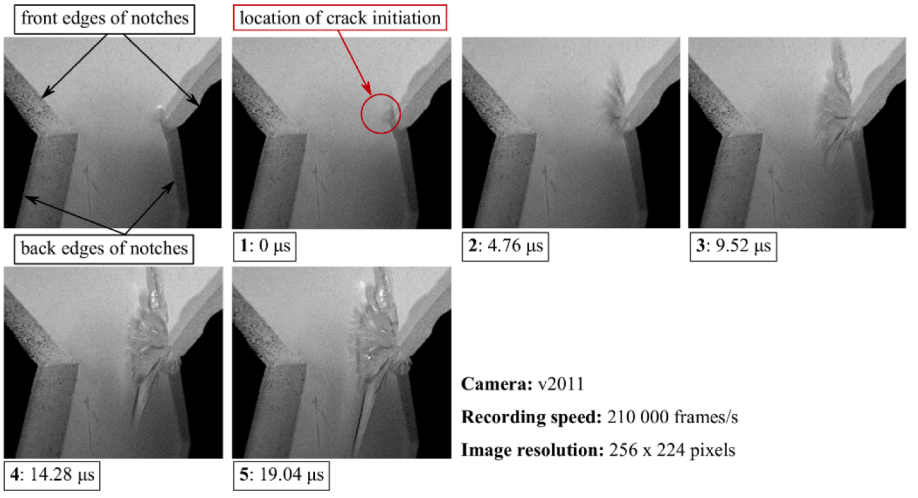


**Fig. 27.** Crack propagation during torsion in a notched specimen (S 0.5–3-5) with notch root radius $\rho = 0.5$ mm and nominal thickness $g = 5$ mm.

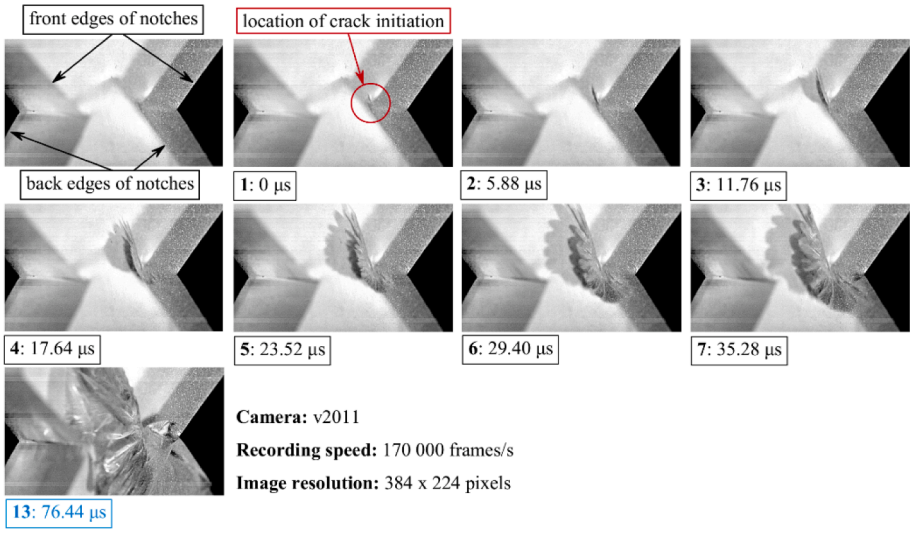


**Fig. 28.** Crack propagation during torsion in a notched specimen (S 0.5–1-15) with notch root radius $\rho = 0.5$ mm and nominal thickness $g = 15$ mm.

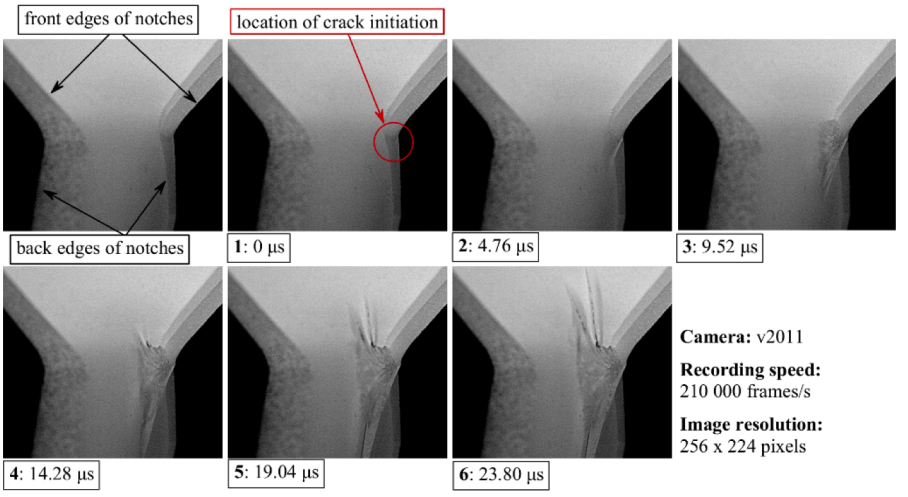


**Fig. 29.** Crack propagation during torsion in a notched specimen (S 2–2-5) with notch root radius $\rho = 2$ mm and nominal thickness $g = 5$ mm.

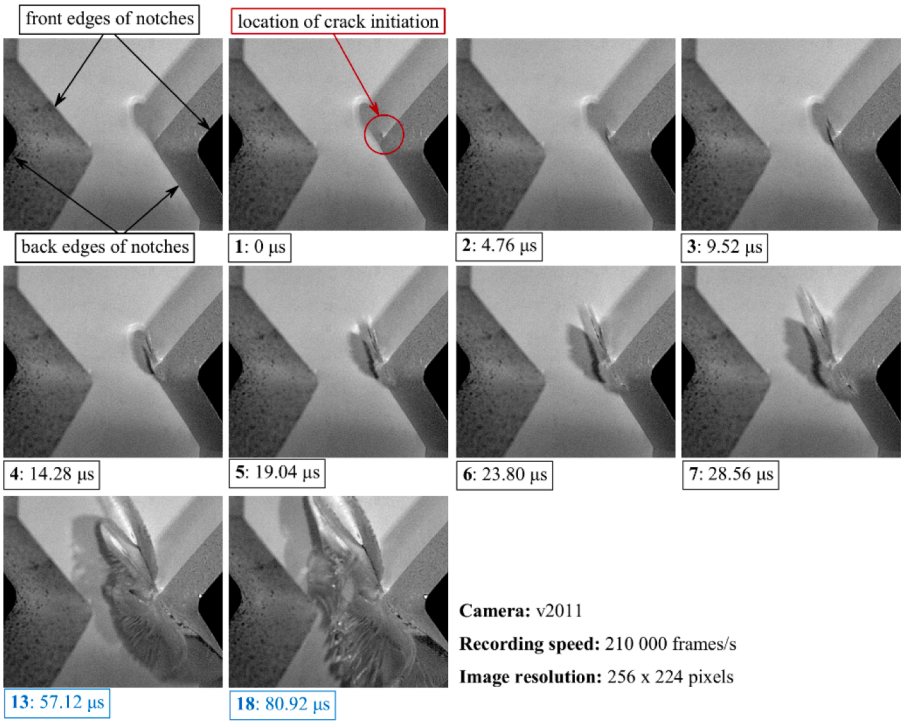


**Fig. 30.** Crack propagation during torsion in a notched specimen (S 2–2-15) with notch root radius $\rho = 2$ mm and nominal thickness $g = 15$ mm.

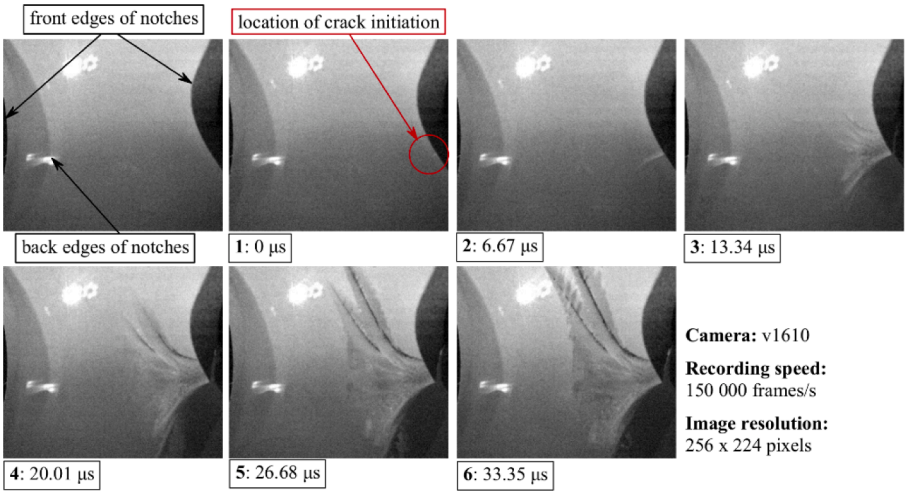


**Fig. 31.** Crack propagation during torsion in a notched specimen (S 10–3-5) with notch root radius $\rho = 10$ mm and nominal thickness $g = 5$ mm.

The type of loading affects the crack initiation angle. For the tensile tests crack always appeared near the notch bottom and the crack initiation angle was found to be close to 0°, i.e. the crack initiated in the plane of symmetry of the specimen, normal to the direction of loading. A different situation was observed during the torsion tests. The larger the notch root radius, the smaller the crack initiation angle. For specimens with radius $\rho = 2$ mm, the crack initiation angle $\vartheta_0$ was close to 40° while for $\rho = 10$ mm, $\vartheta_0$ was about equal to 30°. It can be concluded that during torsion tests, the notch root radius, affects the crack initiation angle – the larger the notch root radius, the smaller the crack initiation angle.

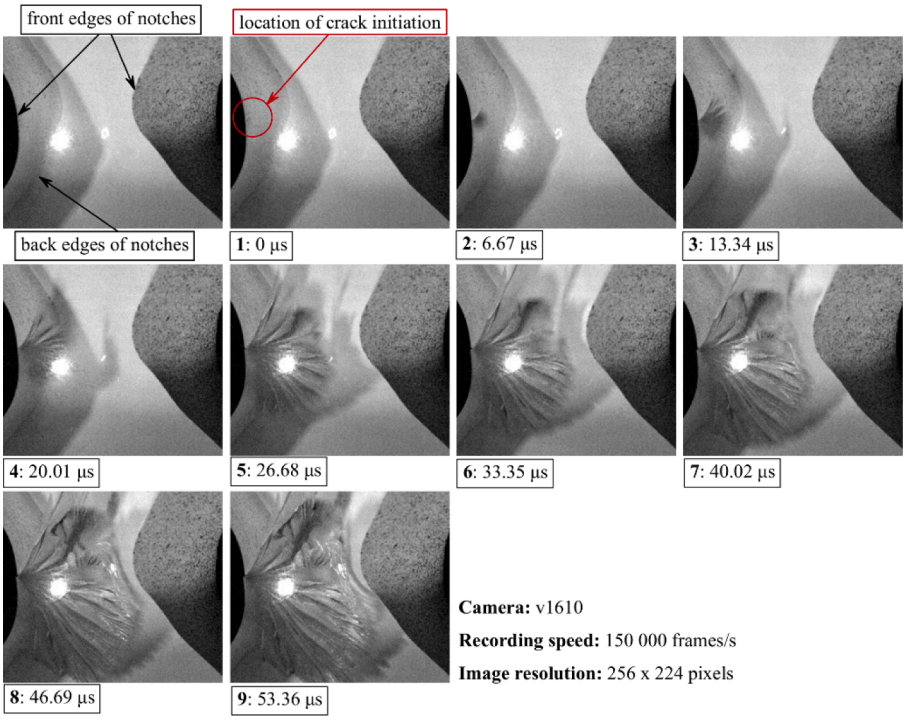


**Fig. 32.** Crack propagation during torsion in a notched specimen (S 10–3-15) with notch root radius $\rho = 10$ mm and nominal thickness $g = 15$ mm.

## Declaration of Competing Interest

The authors declare that they have no known competing financial interests or personal relationships that could have appeared to influence the work reported in this paper.

## Data availability

Data will be made available on request.

## Acknowledgment

This research was funded by the National Science Centre Poland based on project no 2019/33/N/ST8/02382.

## References

[1] A. Seweryn, Brittle fracture criterion for structures with sharp notches, Eng. Fract. Mech. 47 (5) (Mar. 1994) 673–681, https://doi.org/10.1016/0013-7944(94)90158-9.
[2] M.R. Ayatollahi, A.R. Torabi, Brittle fracture in rounded-tip V-shaped notches, Mater. Des. 31 (1) (Jan. 2010) 60–67, https://doi.org/10.1016/j.matdes.2009.07.017.
[3] B.P. Gearing, L. Anand, Notch-sensitive fracture of polycarbonate, Int. J. Solids Struct. 41 (3–4) (Feb. 2004) 827–845, https://doi.org/10.1016/j.ijsolstr.2003.09.058.
[4] A.R. Torabi, B. Saboori, A. Hashemi, Pure mode III fracture of U-notched specimens made of PMMA and GPPS polymers: Experimental and theoretical evaluations, Eng. Fract. Mech. 211 (Apr. 2019) 70–81, https://doi.org/10.1016/j.engfracmech.2019.02.010.
[5] A.R. Torabi, S. Shahbaz, S. Cicero, M.R. Ayatollahi, Fracture testing and estimation of critical loads in a PMMA-based dental material with nonlinear behavior in the presence of notches, Theor. Appl. Fract. Mech. 118 (Apr. 2022), 103282, https://doi.org/10.1016/j.tafmec.2022.103282.
[6] E. Bura, A. Seweryn, Mode I fracture in PMMA specimens with notches – Experimental and numerical studies, Theor. Appl. Fract. Mech. 97 (Oct. 2018) 140–155, https://doi.org/10.1063/1.4992645.
[7] M.R. Ayatollahi, M. Rashidi Moghaddam, S.M.J. Razavi, F. Berto, Geometry effects on fracture trajectory of PMMA samples under pure mode-I loading, Eng. Fract. Mech. 163 (Sep. 2016) 449–461, https://doi.org/10.1016/j.engfracmech.2016.05.014.
[8] A. Leite, V. Mantič, F. París, Crack onset in stretched open hole PMMA plates considering linear and non-linear elastic behaviours, Theor. Appl. Fract. Mech. 114 (Aug. 2021), 102931, https://doi.org/10.1016/j.tafmec.2021.102931.
[9] A. Doitrand, G. Molnár, D. Leguillon, E. Martin, N. Carrère, Dynamic crack initiation assessment with the coupled criterion, Eur. J. Mech. A. Solids 93 (May 2022), 104483, https://doi.org/10.1016/j.euromechsol.2021.104483.
[10] F. Zhou, J.-F. Molinari, T. Shioya, A rate-dependent cohesive model for simulating dynamic crack propagation in brittle materials, Eng. Fract. Mech. 72 (9) (Jun. 2005) 1383–1410, https://doi.org/10.1016/j.engfracmech.2004.10.011.
[11] I. Smirnov, N. Kazarinov, Y. Petrov, Experimental observation and numerical modelling of unstable behaviour of a fast crack velocity, Theor. Appl. Fract. Mech. 101 (Jun. 2019) 53–58, https://doi.org/10.1016/j.tafmec.2019.02.006.

[12] H.J. Sutherland, Acoustical determination of the shear relaxation functions for polymethyl methacrylate and Epon 828-Z, J. Appl. Phys. 49 (7) (Jul. 1978) 3941–3945, https://doi.org/10.1063/1.325403.
[13] G. Destgeer, et al., Acoustic impedance-based manipulation of elastic microspheres using travelling surface acoustic waves, RSC Adv 7 (36) (2017) 22524–22530, https://doi.org/10.1039/C7RA01168G.
[14] F. Berto, M. Elices, P. Lazzarin, M. Zappalorto, Fracture behaviour of notched round bars made of PMMA subjected to torsion at room temperature, Eng Fract Mech 90 (Aug. 2012) 143–160, https://doi.org/10.1016/j.engfracmech.2012.05.001.
[15] F. Berto, D.A. Cendon, P. Lazzarin, M. Elices, Fracture behaviour of notched round bars made of PMMA subjected to torsion at −60°C, Eng. Fract. Mech. 102 (Apr. 2013) 271–287, https://doi.org/10.1016/j.engfracmech.2013.02.011.
[16] S. Liu, Y.J. Chao, X. Zhu, Tensile-shear transition in mixed mode I/III fracture, Int. J. Solids Struct. 41 (22–23) (Nov. 2004) 6147–6172, https://doi.org/10.1016/j.ijsolstr.2004.04.044.
[17] M.R. Ayatollahi, B. Saboori, A new fixture for fracture tests under mixed mode I/III loading, Eur. J. Mech. A. Solids 51 (May 2015) 67–76, https://doi.org/10.1016/j.euromechsol.2014.09.012.
[18] S. Safaei, M.R. Ayatollahi, B. Saboori, Fracture behavior of GPPS brittle polymer under mixed mode I/III loading, Theor. Appl. Fract. Mech. 91 (Oct. 2017) 103–115, https://doi.org/10.1016/j.tafmec.2017.04.017.
[19] P. Poapongsakorn, A. Wiangkham, P. Aengchuan, N. Noraphaiphipaksa, C. Kanchanomai, Time-dependent fracture of epoxy resin under mixed-mode I/III loading, Theor. Appl. Fract. Mech. 106 (Apr. 2020), 102445, https://doi.org/10.1016/j.tafmec.2019.102445.
[20] A.R. Torabi, B. Saboori, S.K. Mohammadian, M.R. Ayatollahi, Brittle failure of PMMA in the presence of blunt V-notches under combined tension-tear loading: Experiments and stress-based theories, Polym Test 72 (Dec. 2018) 94–109, https://doi.org/10.1016/j.polymertesting.2018.10.002.
[21] B. Saboori, A.R. Torabi, S. Keshavarz Mohammadian, Experimental and stress-based theoretical studies on mixed mode I/III fracture of round-tip V-notched Polystyrene specimens, Theor. Appl. Fract. Mech. 95 (Jun. 2018) 283–305, https://doi.org/10.1016/j.tafmec.2018.03.008.
[22] B. Saboori, A.R. Torabi, M.R. Ayatollahi, F. Berto, Experimental verification of two stress-based criteria for mixed mode I/III brittle fracture assessment of U-notched components, Eng. Fract. Mech. 182 (Sep. 2017) 229–244, https://doi.org/10.1016/j.engfracmech.2017.06.005.
[23] F. Hatami, M.R. Ayatollahi, A.R. Torabi, Limit curves for brittle fracture in key-hole notches under mixed mode I/III loading based on stress-based criteria, Eur. J. Mech. A. Solids 85 (Jan. 2021), 104089, https://doi.org/10.1016/j.euromechsol.2020.104089.
[24] M.R. Ayatollahi, A.R. Torabi, Investigation of mixed mode brittle fracture in rounded-tip V-notched components, Eng Fract Mech 77 (16) (Nov. 2010) 3087–3104, https://doi.org/10.1016/j.engfracmech.2010.07.019.
[25] A.R. Torabi, B. Bahrami, M.R. Ayatollahi, Mixed mode I/II brittle fracture in V-notched Brazilian disk specimens under negative mode I conditions, Phys. Mesomech. 19 (3) (Jul. 2016) 332–348, https://doi.org/10.1134/S1029959916030115.
[26] M.R. Ayatollahi, A.R. Torabi, A.S. Rahimi, Brittle fracture assessment of engineering components in the presence of notches: a review, Fatigue Fract. Eng. Mater. Struct. 39 (3) (Mar. 2016) 267–291, https://doi.org/10.1111/ffe.12379.
[27] A.R. Torabi, S. Etesam, A. Sapora, P. Cornetti, Size effects on brittle fracture of Brazilian disk samples containing a circular hole, Eng. Fract. Mech. 186 (Dec. 2017) 496–503, https://doi.org/10.1016/j.engfracmech.2017.11.008.
[28] A.R. Torabi, S.M. Abedinasab, Brittle fracture in key-hole notches under mixed mode loading: Experimental study and theoretical predictions, Eng. Fract. Mech. 134 (Jan. 2015) 35–53, https://doi.org/10.1016/j.engfracmech.2014.12.006.
[29] H. Majidi, M. Ayatollahi, A. Torabi, A. Zaheri, Energy-based assessment of brittle fracture in VO-notched polymer specimens under combined compression-shear loading conditions, Int. J. Damage Mech 28 (5) (May 2019) 664–689, https://doi.org/10.1177/1056789518780424.
[30] M.R. Ayatollahi, M.R.M. Aliha, M.M. Hassani, Mixed mode brittle fracture in PMMA—An experimental study using SCB specimens, Mater. Sci. Eng. A 417 (1–2) (Feb. 2006) 348–356, https://doi.org/10.1016/j.msea.2005.11.002.
[31] B. Bahrami, M.R. Ayatollahi, I. Sedighi, M.A. Pérez, A.A. Garcia-Granada, The effect of in-plane layer orientation on mixed-mode I-II fracture behavior of 3D-printed poly-carbonate specimens, Eng. Fract. Mech. 231 (May 2020), 107018, https://doi.org/10.1016/j.engfracmech.2020.107018.
[32] B. Ameri, F. Taheri-Behrooz, M.R.M. Aliha, Fracture loads prediction of the modified 3D-printed ABS specimens under mixed-mode I/II loading, Eng. Fract. Mech. 235 (Aug. 2020), 107181, https://doi.org/10.1016/j.engfracmech.2020.107181.
[33] E. Bura, Ł. Derpeński, A. Seweryn, Fracture in PMMA notched specimens under compression – Experimental study, Polym. Test 77 (Aug. 2019), 105923, https://doi.org/10.1016/j.polymertesting.2019.105923.
[34] A.R. Torabi, K. Hamidi, B. Shahbazian, S. Cicero, F. Berto, Extension of the Equivalent Material Concept to Compressive Loading: Combination with LEFM Criteria for Fracture Prediction of Keyhole Notched Polymeric Samples, Appl. Sci. 11 (9) (Apr. 2021) 4138, https://doi.org/10.3390/app11094138.
[35] A.R. Torabi, K. Hamidi, A.S. Rahimi, S. Cicero, Notch Fracture in Polymeric Specimens under Compressive Stresses: The Role of the Equivalent Material Concept in Estimating the Critical Stress of Polymers, Appl. Sci. 11 (5) (Feb. 2021) 2104, https://doi.org/10.3390/app11052104.
[36] E. Bura, A. Seweryn, Fracture Initiation in Notched Specimens Subjected to Compression: Strain Rate Effect, Materials 13 (11) (Jun. 2020) 2613, https://doi.org/10.3390/ma13112613.
[37] S. Kim, P.A. Wilson, Z.-M. Chen, Large-eddy simulation of the turbulent near wake behind a circular cylinder: Reynolds number effect, Appl. Ocean Res. 49 (Jan. 2015) 1–8, https://doi.org/10.1016/j.apor.2014.10.005.
[38] M. Bai, H. Yin, J. Zhao, Y. Li, Y. Yang, Y. Wu, Application of PMMA bone cement composited with bone-mineralized collagen in percutaneous kyphoplasty, Regen Biomater 4 (4) (Aug. 2017) 251–255, https://doi.org/10.1093/rb/rbx019.
[39] G.R. Mitchell, "X-Ray Scattering from Non-crystalline and Liquid Crystalline Polymers", in *Comprehensive Polymer Science and Supplements*, Elsevier, 1989, pp. 687–729.
[40] B.D. Ratner, "Polymeric Implants", in *Polymer Science: A Comprehensive Reference*, Elsevier (2012) 397–411, https://doi.org/10.1016/B978-0-444-53349-4.00230-2.
[41] Y. Koike, K. Koike, "Optical Fibers", in *Polymer Science: A Comprehensive Reference*, Elsevier (2012) 283–304, https://doi.org/10.1016/B978-0-444-53349-4.00209-0.
[42] W. Macek, G. Robak, K. Żak, R. Branco, Fracture surface topography investigation and fatigue life assessment of notched austenitic steel specimens, Eng Fail Anal 135 (May 2022), 106121, https://doi.org/10.1016/j.engfailanal.2022.106121.
[43] T. Kobayashi, D.A. Shockey, Fracture surface topography analysis (FRASTA)—Development, accomplishments, and future applications, Eng. Fract. Mech. 77 (12) (Aug. 2010) 2370–2384, https://doi.org/10.1016/j.engfracmech.2010.05.016.
[44] A. Seweryn, Z. Mróz, A non-local stress failure condition for structural elements under multiaxial loading, Eng. Fract. Mech. 51 (6) (1995) 955–973, https://doi.org/10.1016/0013-7944(94)00335-F.
[45] A. Seweryn, A non-local stress and strain energy release rate mixed mode fracture initiation and propagation criteria, Eng. Fract. Mech. 59 (6) (1998) 737–760, https://doi.org/10.1016/S0013-7944(97)00175-6.
[46] L. Derpenski, A. Seweryn, Ductile fracture of EN-AW 2024 aluminum alloy specimens with notches under biaxial loading. Part 1 – Experimental research, Theor. Appl. Fract. Mech. 84 (2016) 192–202, https://doi.org/10.1016/j.tafmec.2016.06.007.
[47] L. Derpenski, A. Seweryn, Ductile fracture of EN-AW 2024 aluminum alloy specimens with notches under biaxial loading. Part 2 – Numerical research and ductile fracture criterion, Theor. Appl. Fract. Mech. 84 (2016) 203–214, https://doi.org/10.1016/j.tafmec.2016.06.008.
[48] Z. Mróz and A. Seweryn, "Damage description with related crack initiation and propagation conditions," in *Journal De Physique. IV : JP*, 1996, vol. 6, no. 6. doi: 10.1051/jp4:1996653.